The single *Drosophila* ZO-1 protein Polychaetoid regulates embryonic morphogenesis in coordination with Canoe/afadin and Enabled

Wangsun Choi[a], Kuo-Chen Jung[a], Kevin S. Nelson[b], Manzoor A. Bhat[c,d], Greg J. Beitel[b], Mark Peifer[a,e], and Alan S. Fanning[c,e]

[a]Department of Biology, University of North Carolina at Chapel Hill, Chapel Hill, NC 27599; [b]Department of Molecular Biosciences, Northwestern University, Evanston, IL 60208; [c]Department of Cell and Molecular Physiology, University of North Carolina at Chapel Hill, Chapel Hill, NC 27599; [d]Curriculum in Neurobiology and UNC-Neuroscience Center, University of North Carolina at Chapel Hill, Chapel Hill, NC 27599; [e]Lineberger Comprehensive Cancer Center, University of North Carolina at Chapel Hill, Chapel Hill, NC 27599

ABSTRACT **Adherens and tight junctions play key roles in assembling epithelia and maintaining barriers. In cell culture zonula occludens (ZO)–family proteins are important for assembly/maturation of both tight and adherens junctions (AJs). Genetic studies suggest that ZO proteins are important during normal development, but interpretation of mouse and fly studies is limited by genetic redundancy and/or a lack of null alleles. We generated null alleles of the single *Drosophila* ZO protein Polychaetoid (Pyd). Most embryos lacking Pyd die with striking defects in morphogenesis of embryonic epithelia including the epidermis, segmental grooves, and tracheal system. Pyd loss does not dramatically affect AJ protein localization or initial localization of actin and myosin during dorsal closure. However, Pyd loss does affect several cell behaviors that drive dorsal closure. The defects, which include segmental grooves that fail to retract, a disrupted leading edge actin cable, and reduced zippering as leading edges meet, closely resemble defects in *canoe* zygotic null mutants and in embryos lacking the actin regulator Enabled (Ena), suggesting that these proteins act together. Canoe (Cno) and Pyd are required for proper Ena localization during dorsal closure, and strong genetic interactions suggest that Cno, Pyd, and Ena act together in regulating or anchoring the actin cytoskeleton during dorsal closure.**

Monitoring Editor
Alpha Yap
University of Queensland

Received: Dec 28, 2010
Revised: Apr 1, 2011
Accepted: Apr 8, 2011

INTRODUCTION

Epithelia, which in their simplest form are single-cell-thick sheets of cells, are among the most common tissue architectures. They form barriers insulating the body from the external environment and create biochemically distinct tissue spaces required for organ function. Individual cells are joined by cadherin-based adherens junctions (AJs), whereas movement of ions, macromolecules, and lymphocytes between cells is regulated by tight junctions (TJs) or their analogues (Nelson, 2008). Cadherin-based cell adhesion also plays a key role in initial polarization of cells during embryogenesis and helps modulate adhesion during morphogenetic movements like gastrulation, which reshape the body plan (Harris *et al*., 2009).

AJs are conserved throughout animals, assembling around transmembrane cadherins that provide the adhesive component (Nelson, 2008). Cadherins bind cytoplasmic β- and α-catenin, which regulate cytoskeletal interactions and help signal cells that adhesion has occurred. TJs per se are less broadly conserved, although most animals have a paracellular barrier (Furuse and Tsukita, 2006). In *Drosophila*, for example, the barrier involves septate junctions. In both vertebrates and insects, claudin family tetraspan transmembrane proteins are critical structural components of the barrier (Furuse and Tsukita, 2006). Mammalian claudins are organized into

This article was published online ahead of print in MBoC in Press (http://www.molbiolcell.org/cgi/doi/10.1091/mbc.E10-12-1014) on April 20, 2011.

Address correspondence to: Mark Peifer (peifer@unc.edu), Alan Fanning (Alan_Fanning@med.unc.edu).

Abbreviations used: Abl, Abelson; AJ, adherens junction; AJC, adherens junction complex; AP, anterior–posterior; Arm, armadillo; AS, amnioserosa; Cno, canoe; DB, dorsal branch; Df, deficiency; Dpp, decapentaplegic; DSRF, *Drosophila* serum response factor; DT, dorsal trunk; DV, dorsal ventral; Ed, echinoid; Ena, enabled; FLP, flippase; FRT, flippase recognition target; GFP, green fluorescent protein; LE, leading edge; Myo, myosin; MZ, maternal and zygotic; Pyd, polychaetoid; SJ, septate junction; Su(dx), suppressor of deltex; TJ, tight junction; Verm, vermiform; ZO, zonula occludens.

strands circumscribing the apical margin of epithelial cells and, analogous to cadherins, form homotypic adhesive complexes between adjacent cells. In mammals, physiological characteristics of different epithelia are determined, in part, by which of 25+ claudins are expressed (Anderson and Van Itallie, 2009).

Claudins, like cadherins, bind cytosolic proteins that regulate assembly into the apical junction complex (AJC) and association with the actin cytoskeleton (Anderson and Van Itallie, 2009; Furuse, 2010). In mammals, the most important are the multidomain scaffolding proteins zonula occludens (ZO)-1 and ZO-2 (Fanning and Anderson, 2009). They bind all known transmembrane TJ proteins (claudin, occludin, and junctional adhesion molecule [JAM]) and many signaling molecules regulating TJ assembly (e.g., Gα12, PLCβ3, cdc42 GEF Tuba). They also bind directly to F-actin and other cytoskeletal proteins (e.g., Shroom2 and cortactin). Although ZO-1 and ZO-2 are somewhat redundant in cultured cells, cells lacking both proteins do not assemble TJ proteins into the AJC and fail to form a paracellular barrier (Umeda *et al.*, 2006). In addition, apical actin and myosin are altered (McNeil *et al.*, 2006; Ikenouchi *et al.*, 2007). Thus ZO proteins may not simply regulate assembly of proteins like claudin into the barrier, but they may also integrate claudin barrier assembly with regulation of the apical actomyosin cytoskeleton.

Of interest, TJ formation depends on AJs by mechanisms that are still poorly understood—disruption of E-cadherin–mediated cell adhesion using antibodies or calcium depletion triggers reversible disassembly of the TJ barrier (Gumbiner *et al.*, 1988). Conversely, several TJ proteins are also AJ components. For example, ZO-1 and ZO-2 are components of AJs in nonmuscle cells and, like JAM and PAR-3, localize to early cadherin-based cell–cell contacts in epithelia (Yonemura *et al.*, 1995; Suzuki *et al.*, 2002). Of interest, ZO-1 and ZO-2 also bind many AJ proteins, including α-catenin, p120ctn, and AF-6/afadin (Fanning and Anderson, 2009). In fact, culture-based assays suggest that ZO-1 and ZO-2 can promote AJ assembly, cell–cell adhesion, and organization of the cortical actin belt associated with AJs (Imamura *et al.*, 1999; Ikenouchi *et al.*, 2007; Yamazaki *et al.*, 2008). These observations led to the hypothesis that ZO-1 and ZO-2 play a role in AJ assembly, possibly by regulating cytoskeletal dynamics at the zonula adherens.

Drosophila has a single ZO family member, Polychaetoid (Pyd). *pyd* mutants were originally described in 1935 (Lindsley and Zimm, 1992) as one of many mutations affecting development of adult mechanosensory bristles. *pyd* mutants have excess bristles, a result of altered cell fate choices controlled by achaete-scute family basic helix-loop-helix transcription factors (Chen *et al.*, 1996; Takahisa *et al.*, 1996). Pyd also regulates eye development, as *pyd* mutants have altered numbers of cells taking on cone cell, primary pigment cell, or photoreceptor fates (Chen *et al.*, 1996; Seppa *et al.*, 2008). In embryos, Pyd plays a role in development of the tracheal system (Jung *et al.*, 2006), influencing both cell fate choices, as in sensory organs, and cell rearrangements, as in the developing eye. Genetic interaction studies suggest that Pyd regulates or works in parallel with Notch (Chen *et al.*, 1996; Takahisa *et al.*, 1996), Dpp/BMP (Seppa *et al.*, 2008), and c-Jun NH_2-terminal kinase (JNK) (Takahashi *et al.*, 1998) signaling.

Given these striking effects on cell fate determination, it was thus initially somewhat surprising when *pyd* was found to encode the single fly ZO family member (Takahisa *et al.*, 1996). Furthermore, in most embryonic and larval tissues Pyd primarily colocalizes with AJ proteins DE-cadherin (DE-cad) and Armadillo (Arm; fly β-catenin) rather than with septate junction proteins (Takahashi *et al.*, 1998; Wei and Ellis, 2001; Jung *et al.*, 2006; Seppa *et al.*, 2008; Sawyer *et al.*, 2009). This led to the hypothesis, as yet untested, that Pyd might be critical for cadherin-based adhesion or signaling.

Among the binding partners of both mammalian and fly ZO-1 is afadin/Canoe (Cno) (also known as AF-6; Yamamoto *et al.*, 1997; Takahashi *et al.*, 1998), an actin-binding protein that localizes to AJs, binds the cytoplasmic tail of nectins, and is an effector of the Ras family GTPase Rap1 (Takai *et al.*, 2008; Boettner and Van Aelst, 2009). Both Pyd and Cno localize to embryonic AJs, and they genetically interact during *Drosophila* embryogenesis (Takahashi *et al.*, 1998). Like *pyd*, *cno* genetically interacts with Notch pathway mutants, and both affect cell fate choice in the fly eye (Miyamoto *et al.*, 1995). Both *pyd* and *cno* also genetically interact with the JNK pathway (Takahashi *et al.*, 1998). These and other data led to the suggestion that these PDZ-domain proteins might act as scaffolds for signal transduction at AJs. However, both also affect cell behavior more directly. Cno regulates cell shape change during dorsal closure (Miyamoto *et al.*, 1995; Takahashi *et al.*, 1998; Boettner *et al.*, 2003), and genetic interactions with *pyd* enhance the effects of *cno* mutations during this process (Takahashi *et al.*, 1998). Cno also plays a critical role in regulating linkage between AJs and the cortical actin cytoskeleton during apical constriction (Sawyer *et al.*, 2009), whereas Pyd regulates cell adhesion and cell shape change during fly eye development (Seppa *et al.*, 2008). Pyd RNAi knockdown elevates DE-cadherin and the nectin-like protein Roughest at AJs, and *pyd* genetically interacts with mutations in the genes encoding them. These observations suggest that Cno and Pyd regulate similar aspects of morphogenesis.

Genetic analysis in mice, worms, and flies illustrated important roles for ZO family members in development. In *Caenorhabditis elegans* the single ZO-1 homologue *zoo-1* plays an important but not fully essential role in embryonic morphogenesis (Lockwood *et al.*, 2008). RNAi knockdown leads to partially penetrant embryonic lethality, with defects in body elongation following ventral enclosure. Genetic interactions suggest that nematode ZO-1 reinforces junctions against actomyosin-based contractility, working together with the cadherin–catenin complex to stabilize junctional actin.

In the mouse, after fertilization, ZO-1 and ZO-2 localize to cadherin-based cell–cell contacts and segregate to TJs following compaction (Eckert and Fleming, 2008). Thus one might predict that they would be very early lethals, like E-cadherin mutants (Larue *et al.*, 1994; Riethmacher *et al.*, 1995), but this is not the case. Embryos lacking ZO-2 show the first defects at E6.5, much later than E-cadherin mutants, and fail to complete gastrulation (Xu *et al.*, 2008). However, this phenotype is likely to reflect an essential role in the extraembryonic tissues, since ZO-2 mutant cells can contribute to most or all tissues in chimeric embryos, with up to 95% of cells in a tissue lacking ZO-2 (Xu *et al.*, 2009). Embryos lacking ZO-1 show abnormalities significantly later (E8.5), which include delayed growth, increased apoptosis, and defects in formation of the notochord and extraembryonic endoderm (Katsuno *et al.*, 2008). However, as in ZO-2, whether these defects are primary or secondary to defects in extraembryonic tissue remains unclear. Loss of ZO-3 is without apparent phenotype (Adachi *et al.*, 2006). Because cell culture studies suggest that ZO-1 and ZO-2 can act redundantly, the absence of published double mutants leaves the question of the full role of ZO family proteins in mammalian embryogenesis unclear.

The role of *Drosophila* Pyd in embryonic development also remains an open question. Although many *pyd* alleles are adult viable, pyd^{C5} and $pyd^{BG02748}$ homozygotes have significant defects in development of the embryonic tracheal system (Jung *et al.*, 2006). pyd^{C5} and pyd^{J14} have been reported to be at least partially penetrant embryonic lethal (Chen *et al.*, 1996), and the embryonic lethality of pyd^{C5} can be rescued by expression of wild-type Pyd (Wei and Ellis, 2001). However, more recent data suggest that the lethality of

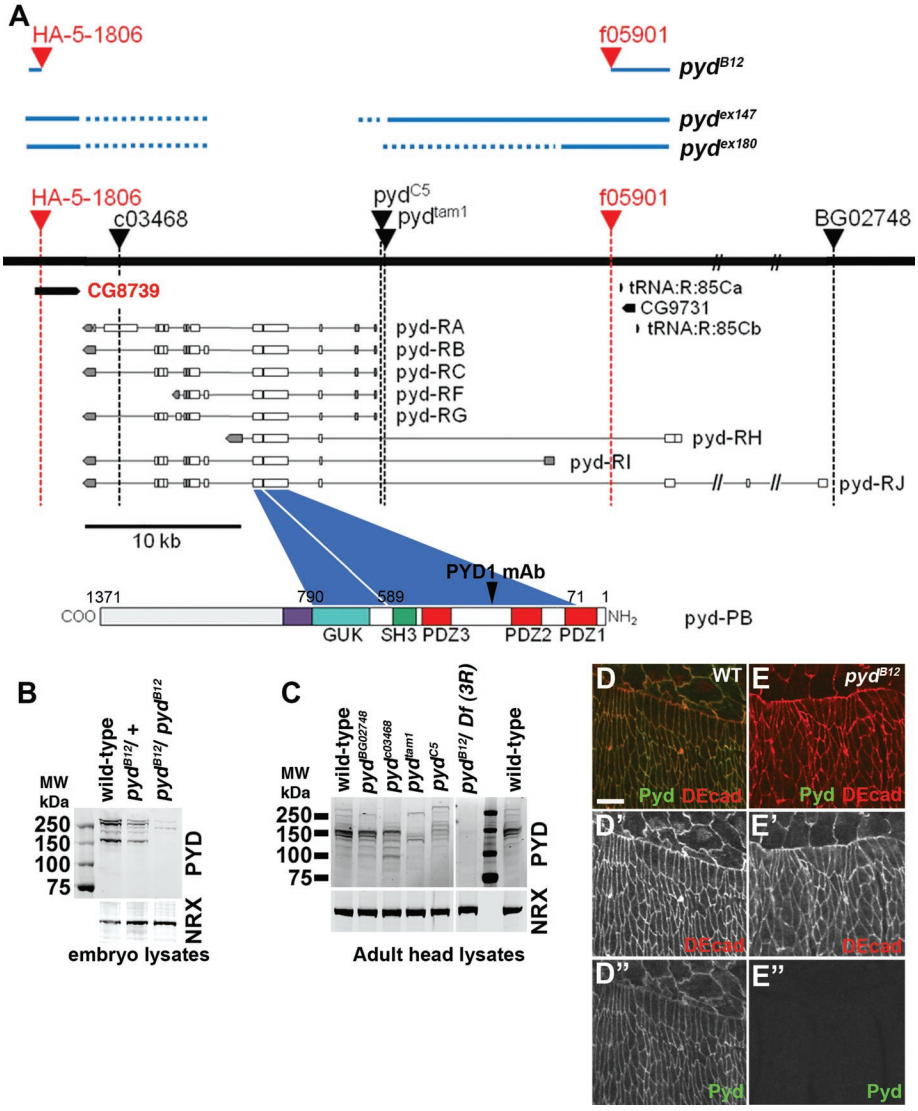

FIGURE 1: Generating a null allele of *pyd*. (A) The black line indicates the relevant genomic region of the right arm of the third chromosome. Immediately above the line are triangles indicating the position of P-element insertions in different *pyd* alleles. Those indicated in red were used to generate the deletion allele, pyd^{B12}; the extent of the resulting deletion is indicated above the black line. The approximate extent of the deletions in pyd^{ex147} and pyd^{ex180}, two additional *pyd* deletion alleles generously provided by Sarah Bray (Djiane *et al.*, 2011), are similarly indicated. Below the black line are diagrammed the many predicted isoforms of *pyd*; the protein domains in one of these, Pyd-PB, are diagrammed at the bottom. We also indicate the coding sequences of two predicted protein-coding genes and two tRNA genes in the region, including CG8739, which is also removed by pyd^{B12}. (B) Protein extracts from embryos of the indicated zygotic genotypes immunoblotted with anti-Pyd. Neurexin (Nrx) is a loading control. Molecular weight markers are indicated. Note that pyd^{B12} mutant embryos were derived from heterozygous mothers, and thus maternally contributed Pyd remains. (C) Protein extracts of adult heads of flies of the indicated genotypes were immunoblotted with anti-Pyd. *Df(3R) = Df(3R)p-XT103.* (D, E) Wild-type and maternal/zygotic pyd^{B12} embryos immunostained for DE-cad and Pyd. Scale bar, 10 μm.

pyd^{C5} is due to closely linked lethal mutations in other genes (Chen *et al.*, 1996; Jung *et al.*, 2006; Seppa *et al.*, 2008). Furthermore, it is not clear whether any of the existing *pyd* alleles are in fact null alleles. The *pyd* gene is complex, with two transcriptional start sites tens of kilobases apart and complex alternative splicing (Figure 1A; www.flybase.org). Many of the best-characterized *pyd* alleles are caused by insertion of P-element transposons in introns or 5′ flanking region and thus do not disrupt coding sequence (Figure 1A). pyd^{C5} was reported to be null for protein expression in embryos (Wei and Ellis, 2001), but pyd^{C5} mutants express normal levels of Pyd protein in the developing eye (Seppa *et al.*, 2008). Thus, as a result of the genetic complexity of the ZO family in mice and the lack of clarity surrounding existing *pyd* alleles in *Drosophila*, the full roles of ZO family members in embryonic morphogenesis remain unclear.

Our interest in mammalian ZO family members and *Drosophila* Cno prompted us to resolve this issue. We hypothesized that Pyd would play an essential role in morphogenesis, regulating adhesion and the cytoskeleton like its mammalian homologues. We tested this hypothesis using a new antibody to Pyd, which recognizes all isoforms, and a definitively null allele of *pyd*, which deletes all of the protein coding sequence.

RESULTS

Generation of a null allele of *pyd* and comparison of Pyd protein levels in different alleles

The *pyd* locus has a complex organization (Figure 1), and several reports have questioned whether the reported phenotypes of some previously characterized P-element insertion alleles at *pyd* result from mutations at other, linked loci (Jung *et al.*, 2006; Seppa *et al.*, 2008). Furthermore, it is unclear to what extent existing alleles affect gene expression at the *pyd* locus. To address these issues, we generated a true *pyd* null allele using FLP-mediated site-specific recombination between two existing P-element insertions (HA-5–1806 and f05901; Figure 1A). The resulting allele, pyd^{B12}, has a 37-kb genomic deletion that eliminates the coding sequence of all known and predicted Pyd isoforms and also deletes an adjacent locus, CG8379, of unknown function (Figure 1A).

We compared Pyd protein expression from our new allele with that from several previously characterized alleles, using extracts from zygotic mutant embryos or adults. We immunoblotted with our newly generated monoclonal antibody (mAb) PYD1, which should recognize all predicted products of the *pyd* locus (Figure 1A, bottom). This antibody recognized overlapping but distinct complex sets of protein isoforms in wild-type embryos (Figure 1B, left lane) and wild-type adult heads (Figure 1C, left lane), consistent with the predicted complex alternative splicing of the locus. In embryos zygotically homozygous for pyd^{B12} but retaining maternally contributed wild-type Pyd (selected by absence of green fluorescent protein [GFP] expression from the Balancer chromosome), we saw strong reduction of Pyd isoforms, whereas heterozygous embryos have reduced accumulation (Figure 1B). In extracts from heads of adult animals, we observed loss of all major immunoreactive

Female	Male	Homozygotes (%)	Heterozygotes (%)	No. of adults
pyd^{B12}/TM3	Df(3R) pXT103/TM3	23[a] (33[b])	77[a] (66[b])	209
pyd^{B12}/TM6	pyd^{B12}/TM6	24 (33)	76 (66)	252
pyd^{B12} /pyd^{B12}	pyd^{B12}/TM3	1[a] (50[b])	99 (50)	893
	pyd^{B12}/TM6	2 (50)	98 (50)	441
	Df(3R) pXT103/TM3	4 (50)	96 (50)	728
	pyd^{ex180}/TM3	23 (50)	77 (50)	893
pyd^{B12}/Df(3R) pXT103	pyd^{B12}/TM3	2 (50)	98 (50)	283
	pyd^{B12}/TM6	3 (50)	97 (50)	307

Crosses were carried out at 25°C.
[a]Actual.
[b]Expected.

TABLE 1: Adult viability of *pyd* alleles.

proteins in hemizygous pyd^{B12} mutants (Figure 1C, pyd^{B12}/Df(3R)). Furthermore, staining of cell junctions by anti-Pyd antibody (Figure 1D) was eliminated in maternal/zygotic pyd^{B12} mutant embryos (Figure 1E). Together, these data confirm antibody specificity and the null nature of the pyd^{B12} allele. In contrast, some of the other previously characterized *pyd* alleles, such as pyd^{C5} and $pyd^{BG02748}$, still have substantial levels of Pyd proteins (Figure 1C). Others, including pyd^{c03468} and pyd^{tam}, had reduced levels of Pyd but clearly retained expression of certain isoforms (Figure 1C). Together, these data suggest that the defects seen in many previously characterized mutants do not reflect the null phenotype and suggest that our new allele serves as a molecular null.

pyd is not an essential gene but its loss substantially reduces viability

Given the apparently essential roles of ZO family members in TJ and AJ assembly or maturation in vitro (see *Introduction*), we hypothesized that a true null allele of *pyd* would also be lethal. To our surprise, we found that pyd^{B12} homozygous or hemizygous [allele over the chromosomal deficiency *Df(3R)-pXT103*] flies are zygotically adult viable, with slightly reduced zygotic viability (23–24% of progeny, as opposed to 33% expected; Table 1). These zygotic mutant adults had bristle defects and rough eyes similar to those seen with previously characterized alleles; we did not characterize these defects further, as they were the subject of a parallel study by Djiane *et al.* (2011). In *Drosophila*, maternally contributed protein can sometimes mask effects on viability. We thus examined viability of homozygous mutant progeny of pyd^{B12} homozygous or hemizygous mothers. In this case, viability was strongly compromised, with mutant animals achieving adulthood at 1–23% of the expected number (Table 1). Thus loss of maternal and zygotic Pyd substantially compromises development.

Complete loss of Pyd leads to partially penetrant embryonic lethality

These data ruled out an essential role for Pyd in zygotic development but indicated that maternally and zygotically mutant animals have very reduced viability. To determine when mutant animals died, we examined the viability of embryos completely lacking maternal and zygotic Pyd. Because pyd^{B12} is adult viable, we could generate maternal and zygotic pyd^{B12} mutant embryos (henceforth called pyd^{MZ}) derived from homozygous mutant mothers and fathers (Table 2). pyd^{MZ} mutant embryos showed 60% embryonic lethality. Maternal and zygotic mutant progeny of mothers heteroallelic for pyd^{B12} and the large deficiency *Df(3R)p-XT103* [pyd^{B12}/*Df(3R) p-XT103* females crossed to pyd^{B12}/TM3 males] also died as embryos (Table 2), in contrast to embryos zygotically mutant for *pyd* [pyd^{B12} or *Df(3R)p-XT103*] but maternally wild type, who were embryonic viable (Table 2). To rule out the possibility that CG8379, an adjacent gene also deleted by pyd^{B12}, accounted for the compromised embryonic viability, we crossed pyd^{B12} to two independently derived *pyd* deletion alleles, pyd^{ex147} and pyd^{ex180}, that only remove the *pyd* coding region and leave CG9731 intact (generously provided by Sarah Bray, University of Cambridge, Cambridge, UK; Djiane *et al.*, 2011) (Figure 1A). We saw substantial embryonic lethality (43–58%) when mothers homozygous for either allele were crossed to pyd^{B12} mutant fathers (Table 2), confirming that CG8379 was not the cause of embryonic lethality. Furthermore, embryos maternally and zygotically mutant for either pyd^{ex147} or pyd^{ex180} also died at rates comparable to those of pyd^{B12} maternal/zygotic embryos (66 and 86% embryonic lethality, respectively). Taken together, these data suggest that Pyd is important for embryogenesis but that embryos can survive in its absence.

Many pyd^{MZ} mutants have defects in embryonic morphogenesis

As a first assessment of the embryonic processes affected by Pyd loss, we examined the cuticles of mutant embryos at the end of

Female	Male	% Embryonic lethal	No. of hatched + dead
pyd^{B12}/pyd^{B12}	pyd^{B12}/pyd^{B12}	60.5	347
pyd^{B12}/Df(3R) pXT103	pyd^{B12}/TM3	47.0	100
pyd^{ex147}/pyd^{ex147}	pyd^{B12}/pyd^{B12}	43.3	358
	pyd^{ex147}/pyd^{ex147}	66.2	264
pyd^{ex180}/pyd^{ex180}	pyd^{B12}/pyd^{B12}	58.2	308
	pyd^{ex180}/pyd^{ex180}	85.7	343
pyd^{B12}/+	pyd^{B12}/+	2.0	100
Df(3R) pXT103/+	pyd^{B12}/+	2.0	100

Crosses were carried out at 25°C.

TABLE 2: Embryonic lethality of *pyd* maternal and zygotic mutants.

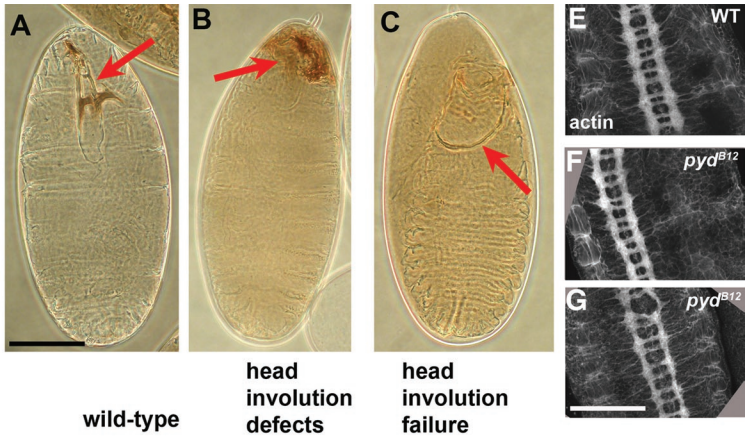

D

Female x male	wild-type	head involution defects	head involution failure	
pyd^{B12} x pyd^{B12}	8%	69%	23%	n=197
pyd^{147} x pyd^{B12}	17%	64%	19%	n=149
pyd^{147} x pyd^{147}	26%	45%	29%	n=154
pyd^{180}x pyd^{B12}	12%	54%	34%	n=121
pyd^{180}x pyd^{180}	17%	32%	51%	n=265

FIGURE 2: pyd^{MZ} mutants have defects in head involution but do not have serious deficits in Notch signaling. (A–C) Cuticles of pyd^{MZ} mutant embryos. (A) Example of wild-type phenotype, with intact head skeleton (arrow). (B) Example of defects in the head skeleton, indicative of defects in head involution. (C) Example of complete failure of head involution. (D) Percentages of dead embryos in each phenotypic class for different allelic combinations of *pyd* alleles. (E–G) Central nervous system revealed by phalloidin staining for actin. pyd^{MZ} mutants do not exhibit obvious nervous system hypertrophy, although some had modest defects in axon architecture (G). Scale bars, 75 µm.

embryogenesis. The cuticle is secreted by epidermal cells and provides a clear readout of cell fate choices and successful completion of morphogenetic movements. In wild-type embryos, cells of the head segments move forward and inward in a process called head involution and then secrete the specialized cuticle of the mouth parts (Figure 2A, arrow). At roughly the same time, lateral sheets of cells of the thoracic and abdominal epidermis move toward the dorsal midline, meeting and zipping closed in a process known as dorsal closure, resulting in an intact dorsal cuticle.

The lethal fraction of pyd^{B12} maternal and zygotic mutants exhibited a characteristic set of cuticle defects consistent with a failure in head involution and minor defects in dorsal closure. We observed no defects indicative of a role of Pyd in anterior–posterior (AP) or dorsal–ventral cell fate choices. In postembryonic development, Pyd plays a role in Notch signaling. *Notch* mutant embryos have a hypertrophied nervous system, and no ventral epidermis, as all ventral ectodermal cells take on neural fates (Poulson, 1940). In contrast, the ventral epidermis is intact in *pyd* maternal/zygotic mutants (Figure 2, A–C), and the CNS is not obviously hypertrophied (Figure 2, E–G). We did, however, note clear defects in morphogenesis. Although some pyd^{MZ} mutants were indistinguishable from wild type (8%—presumably the ~40% of embryos that hatch also had wild-type cuticles; Figure 2D), most mutant embryos (69%) had defects in head involution that resulted in defective head skeletons (Figure 2B, arrow), whereas the most severe (23%) had complete failure of head involution, leading to a hole in the cuticle (Figure 2C, arrow). In addition, some had minor defects in dorsal closure (unpublished data). To confirm that these defects were not due to loss of CG8739 or to another, less closely linked mutation on the pyd^{B12} chromosome, we also examined cuticles of embryos maternally mutant for either pyd^{ex147} or pyd^{ex180}, and zygotically pyd^{147} or pyd^{180} mutant, or transheterozygous for pyd^{B12}. All genotypes exhibited roughly similar percentages of embryos with defects in head involution (Figure 2D). Thus loss of Pyd compromises embryonic morphogenesis, with the strongest defects in head involution, but does not inactivate Notch signaling. The pyd^{MZ} defects are similar in nature, although somewhat less severe, than those we previously observed in *cno* zygotic null mutants (Sawyer *et al.*, 2009).

Pyd is not essential for assembly or maintenance of AJs or for Cno localization to AJs

In addition to their role in TJs, mammalian ZO family proteins play roles in the proper maturation of AJs in cultured cells. To test the hypothesis that Pyd plays a similar role, we examined localization of AJ proteins in pyd^{MZ} null mutants. We found no defects in localization of the epithelial classic cadherin DE-cadherin (Figure 3, A′ vs. B′) or in localization of Armadillo (Arm; fly β-catenin; Figure 3, C′ vs. D′). Even in relatively late mutant embryos, both proteins localized correctly, as did cortical actin, which underlies AJs (Figure 3, A‴ vs. B‴, and unpublished data). We also examined cross sections and found no change in the enrichment of Arm in apical AJs in *pyd* mutants in either the epidermis (Figure 3, H vs. I) or the amnioserosa (Figure 3, J vs. K). Finally, we examined accumulation and localization of Cno (fly afadin), a known AJ protein and Pyd binding partner. Cno levels and localization were also apparently unaffected by Pyd loss (Figure 3, A″ vs. B″). Thus in *Drosophila* the sole ZO family member is not required for assembly or maintenance of AJs.

Loss of Pyd compromises orchestrated cell shape changes in the epidermis during dorsal closure

To explore the cellular roles of Pyd, we explored the characteristic cell shape changes occurring during dorsal closure, and how they shape tissue rearrangements. Dorsal closure begins immediately after germband retraction. During the extended germband stage (stages 9–11), epidermal cells are roughly columnar, with polygonal apical cross sections. During germband retraction (stage 12), the leading edge (LE) cells (those that abut the amnioserosa) become square in apical profile, forming a straight line along the edge of the amnioserosa. As germband retraction is completed, LE cells begin to elongate along the dorsal–ventral (DV) axis (Figure 4, A and K, green arrow) and assemble at their leading edge a cable of actin and nonmuscle myosin II (myosin; Figure 3, C–G). At the same time, amnioserosal cells begin periodic apical constrictions, gradually reducing their apical areas. As constriction proceeds more ventral epidermal cells elongate (Figure 4, C and M, red arrow). Elegant laser surgery experiments demonstrate that apical constriction of amnioserosal cells and constriction of the actomyosin cable both provide the driving force for closure, whereas the epidermis resists elongation, slowing the process (Kiehart *et al.*, 2000). The two leading

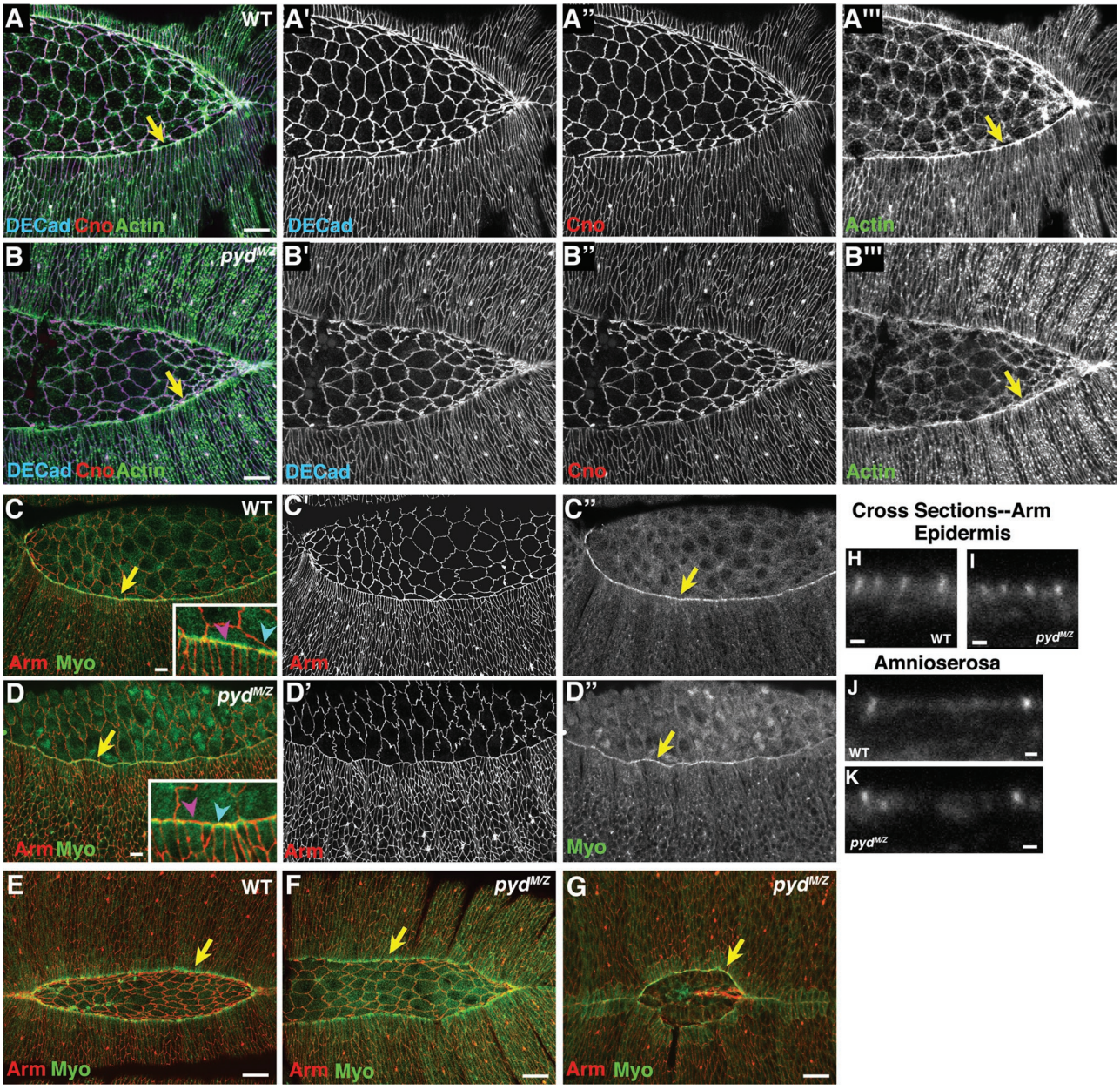

FIGURE 3: *pyd*^{MZ} mutants can assemble and maintain adherens junctions and assemble a leading edge actomyosin cable. Stage 13 or 14 wild-type (WT) or *pyd*^{MZ} mutants, anterior left, dorsal view, antigens indicated. (A, B) Early stage 14. Arrow indicates leading edge actin cable. (C, D) Stage 14. Arrow indicates leading edge myosin cable. Inset, magnified view of leading edge cable. Blue arrowheads, LE cells with constricted leading edges and elevated myosin staining. Magenta arrowheads, LE cells with broadened leading edges and reduced myosin staining. (E–G) Early (E, F) or late (G) stage 14. Arrow indicates leading edge myosin cable. Scale bars, A–G, 10 μm; H–K, 1 μm.

edges meet first at the anterior and posterior ends of the amnioserosa, at structures termed the canthi (Figure 4C, yellow arrows), forming an "eye-shaped" dorsal opening. As the edges meet, cells meet adjoining neighbors from the other side, and the two sheets zip closed (Figure 4, G, M, and P, yellow arrows). Protrusive behavior at the leading edge is required for fully effective zippering (e.g., Woolner *et al.*, 2005; Gates *et al.*, 2007; Millard and Martin, 2008).

The cuticle defects in *pyd*^{MZ} mutants suggested the hypothesis that it plays a role in cell shape changes in dorsal closure. To test this hypothesis, we explored how loss of Pyd affected these orchestrated cell shape changes. *pyd*^{MZ} mutants appeared indistinguishable from wild type through germband retraction (Figure 4, A vs. B). Furthermore, many cellular events of dorsal closure were not precluded. Both LE (Figure 4, L, N, and O, green arrows) and more ventral epidermal cells (Figure 4, N and O, red arrows) were able to elongate, and many did so in a timely manner. Amnioserosal cells also apically constricted roughly on schedule (Figure 4, C vs. D). In a subset of mutants, all the cell shape changes of dorsal closure proceeded in an essentially wild-type manner. However, a substantial majority of mutant embryos had defects in cell shape changes in the epidermis.

In wild-type embryos, LE cells and their more ventral neighbors elongate relatively uniformly, and the widths of their leading edges, where the actomyosin cable assembles, are relatively uniform

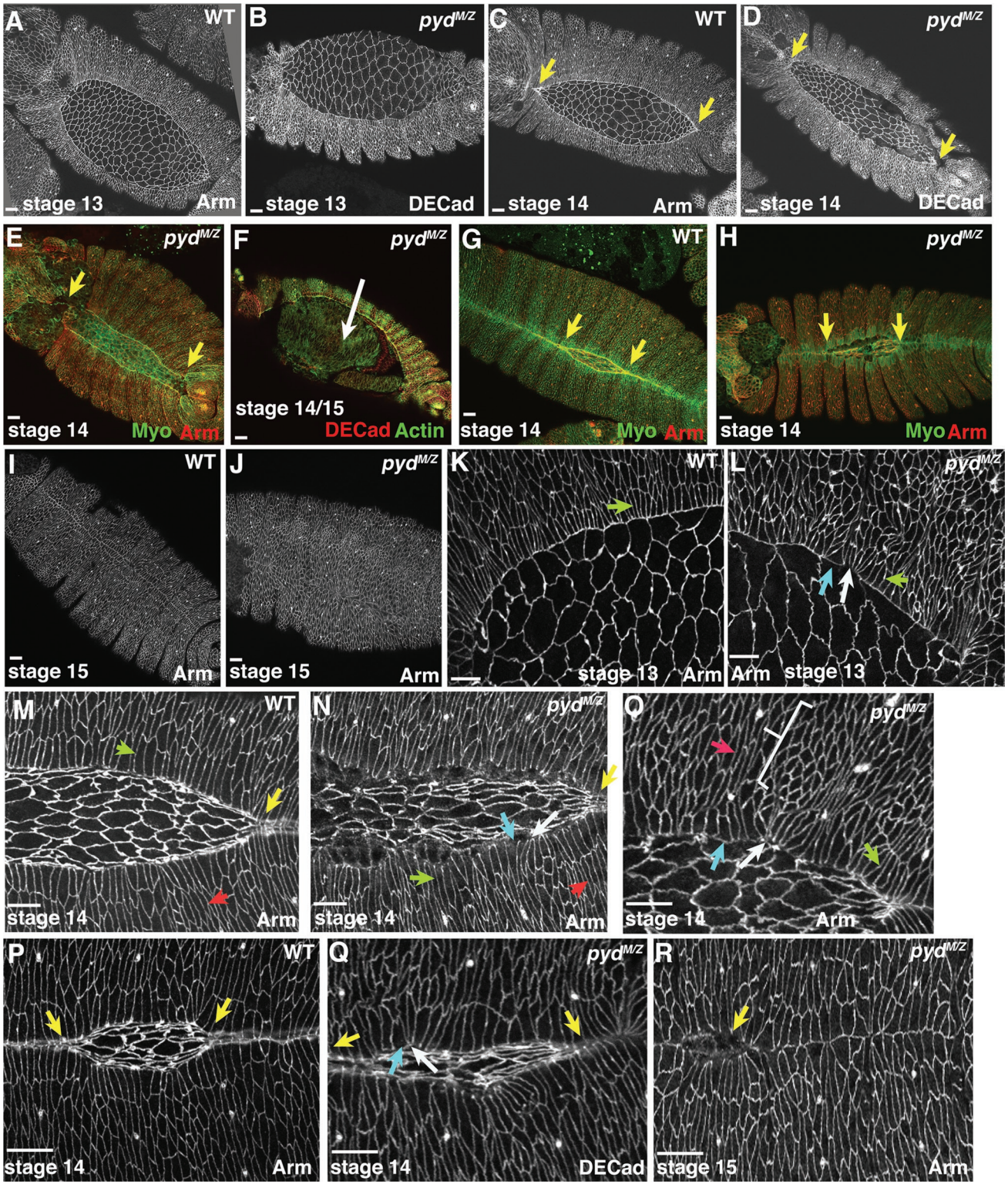

FIGURE 4: *pyd*^{MZ} mutants have defects in LE cell shape and epithelial zippering. Stage 13–15 wild-type (WT) or *pyd*^{MZ} mutants, anterior left, dorsal view, antigens and embryonic stages indicated. (A, B) *pyd*^{MZ} mutants are largely normal through the onset of dorsal closure. (C–E, G, H) *pyd*^{MZ} mutants have apparent defects in zippering at the canthi (yellow arrows), leading to more oval dorsal openings, and also have a wavy leading edge. (F) *pyd*^{MZ} mutant in which dorsal closure failed, leading to exposure of the underlying gut and muscle (arrow) after amnioserosal cell apoptosis. (I, J) Many *pyd*^{MZ} mutants eventually close. (K–R) Close-ups of leading edge and amnioserosa at successively later stages. In *pyd*^{MZ} mutants LE cells retain the ability to elongate (K–O, green arrows), and more lateral epidermal cells can also elongate (M–O, red arrows). However, *pyd*^{MZ} mutants exhibit several defects, including a dorsal opening that is not "eye shaped," a wavy margin of the sheet of epidermal cells, and broadened (L, N, O, and Q, blue arrows) or narrowed (L, N, O, and Q, white arrows) leading edges. In addition, some groups of epidermal cells fail to change shape entirely (O, bracket). Scale bars, 10 μm.

(Figure 4, M and P). As a result, the leading edge of the entire epidermis is quite straight. In contrast, cell shape changes in *pyd*^{MZ} mutants were much less uniform. This became apparent as early as stage 13, when, at the leading edge, some LE cells had very narrow leading edges (Figure 4L, white arrow), suggestive of excess constriction of the leading edge actin cable, whereas in others the leading edge was much broader (Figure 4L, blue arrow), consistent with disruption of the leading edge actin cable. As closure proceeded, these cell shape defects became more widespread. The leading edge of the epidermis was often wavy (Figure 4, N, O, and Q), and LE cells varied from hyperconstricted (Figure 4, N, O, and Q, white arrows) to broadened at the leading edge (Figure 4, N, O, and Q, blue arrows). In addition, groups of cells in the lateral epidermis sometimes failed to change shape at all (Figure 4O, bracket).

To test the hypothesis that these cell shape changes might reflect defects in the actomyosin cable, we examined actin and myosin localization. *pyd*^{MZ} mutants assembled an actin cable at their leading edge at the onset of dorsal closure (Figure 3, A‴ vs. B‴, yellow arrows), despite defects in cell shape. Myosin was also assembled into the leading edge cable in *pyd*^{MZ} mutants (Figure 3, C″ vs. D″, yellow arrows). The cable was maintained in many cells as closure proceeded (Figure 3, E vs. F, yellow arrows) and remained localized to the leading edge even in mutants in which the dorsal opening was highly abnormal in shape (Figure 3, G). However, the intensity of the myosin signal in the cable correlated with LE cell width—cells with constricted leading edges had very strong signals (Figure 3D, inset, blue arrowhead), whereas those with splayed open leading edges had weaker signals (Figure 3D, inset, magenta arrowhead; this was observed to some extent in wild-type cells, where despite the relative uniformity in LE cell width, occasional cells had a splayed open leading edge; Figure 3C, inset). Thus Pyd is not essential for either cable assembly or constriction, but defects in cell shape and the straightness of the leading edge both correlate with defects maintaining the integrity or junctional linkage of the cable.

We next examined zippering of the two epidermal sheets. In wild-type cells, this proceeds from both the posterior and anterior ends, leading to an "eye-shaped" opening in the epidermis (Figure 4, C, G, M, and P, yellow arrows). In contrast, the dorsal openings in *pyd*^{MZ} mutants were often oval shaped (Figure 4, D, H, and N), suggesting that zippering is slowed, as we and others previously observed in mutants in proteins regulating LE protrusive behavior like Rac or Enabled (Ena) (Woolner *et al.*, 2005; Gates *et al.*, 2007). In some cases, failure of the process of head involution resulted in zippering at the anterior canthus being completely prevented (Figure 4E, left arrow). In extreme cases, zippering at the posterior end also seemed largely or completely blocked (Figure 4E, right arrow), whereas in others it was simply slowed substantially (Figure 4, P vs. Q). Thus Pyd promotes zippering together of the two sheets. Although in most cases dorsal closure eventually was completed, cell shapes often remained quite irregular even when the two sheets met, and small regions where the sheets did not seal were retained (Figure 4R). In a subset of embryos, dorsal closure fails and amnioserosal apoptosis leaves a large hole on the dorsal surface, reflecting the holes we occasionally observed in the cuticle (Figure 4F).

To further characterize Pyd's role in dorsal closure, we examined the process live in wild-type and *pyd*^{MZ} mutant embryos, using moesin-GFP to visualize F-actin and cell shapes. Dorsal closure in *pyd*^{MZ} mutants was significantly slower than in wild-type embryos (Figure 5, A vs. B; Video 1 vs. Video 2). To quantify this, we assessed the time required to close, beginning when the greatest distance between the two epidermal sheets was 60 µm. Closure was >50% slower in *pyd*^{MZ} mutants (Figure 5C). Many of the morphogenesis defects we observed in fixed embryos were also readily apparent in our movies. The leading edge was very uneven (Figure 5, A and E, vs. B and F, arrows), and the delay in zippering at the canthi, leading to a more elongated dorsal opening (Figure 5, A vs. B, double-headed arrows), was also apparent in the movies. To quantify the delay in zippering, we measured the rate of zippering from a fixed point representing the position of the anterior canthus when the two epidermal sheets were 60 µm apart. This revealed that the zippering rate was significantly slower in *pyd*^{MZ} mutants (Figure 5D), consistent with the defects we saw in fixed images. Thus Pyd is essential for both the normal kinetics and cellular dynamics of dorsal closure, but the process is robust enough that closure is completed in most embryos in its absence.

Pyd also plays an important role in the resolution of segmental grooves

We observed another striking phenotype in *pyd*^{MZ} mutants that reflects failure of a different cell shape change. In wild-type embryos, one row of epidermal cells per body segment takes on a special cell fate and assumes a different architecture from its neighbors (Larsen *et al.*, 2003; Vincent *et al.*, 2008). These "segmental groove cells" do not elongate like their epidermal neighbors but become almost square in apical cross section. As a result, the chain of segmental groove cells is shorter and thus forms the bottom of a transient groove in the developing epidermis. The grooves begin to retract during germband retraction, as these cells slowly revert to a more "normal" epidermal shape. Thus at the onset of dorsal closure, the grooves remain fairly deep ventrally and come within two to three cell diameters of the leading edge (Figure 6H, red arrows). During the course of dorsal closure, groove cell shapes begin to resemble those of other cells, and segmental grooves gradually become shallower, from dorsal to ventral, and, by the end of dorsal closure, largely disappear (Figure 6, A and E, arrows).

In contrast, we observed that at the end of dorsal closure *pyd*^{MZ} mutants retain very deep segmental grooves; in fact, these are deeper than those seen at any stage of wild-type development, extending deep into the embryo both dorsally (Figure 6, A vs. B) and ventrally (Figure 6, E vs. F, arrows). This defect can be seen as early as the onset of dorsal closure—at this stage wild-type grooves have begun to become shallower and thus end three or so cell diameters from the leading edge (Figure 6H, arrows). In contrast, grooves in *pyd*^{MZ} mutants still extend all the way to the leading edge (Figure 6I; I′ basal is a more basal section showing how deep the abnormal grooves are at this stage). Grooves remain abnormally deep through the end of closure, both in embryos in which closure goes to completion (Figure 6, B and K, arrows) and in those in which it fails completely (Figure 6D, arrows). However, despite these defects, there do not appear to be defects in groove cell specification (e.g., extra cells specified in this fate). Normal groove cells accumulate higher levels of the actin regulator Ena than their neighbors, and only a single row of cells per segment accumulates elevated Ena levels in *pyd*^{MZ} mutants (see later discussion). Thus Pyd is essential for normal relaxation of segmental grooves; the altered tension and cell shapes caused by abnormally deep and persistent segmental grooves are likely to contribute to abnormalities in cell shape at the leading edge.

Pyd is required for proper tracheal development

Previous work showed that zygotic *pyd*^{C5} and *pyd*^{BG02748} mutations perturb morphogenesis of the embryonic tracheal system (Jung *et al.*, 2006). The tracheal system is a network of epithelial tubes that

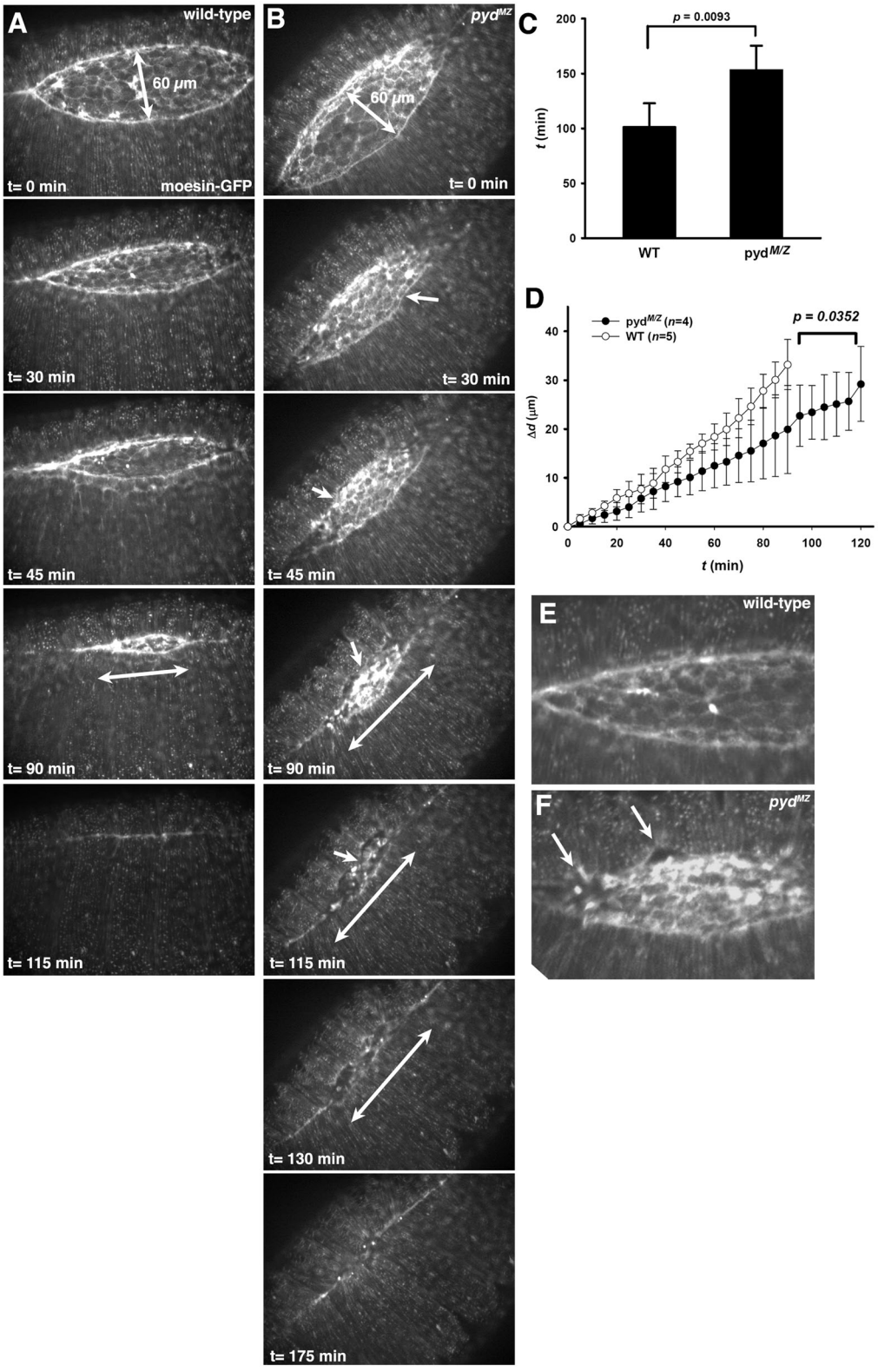

FIGURE 5: Both dorsal closure and zippering are significantly slowed in *pyd*^{MZ} mutants. (A, B) Stills from a movie of representative wild-type or *pyd*^{MZ} mutant embryos expressing the actin-binding domain of moesin fused to GFP (moe-GFP). Videos are included as Supplemental Figure 5A.mov and Supplemental Figure 5B.mov. Times are indicated, beginning when maximum width of the dorsal opening was 60 μm. Double-headed arrows indicate distance between the two canthi, which is reduced by zippering. Arrows in B indicates examples of wavy margin of the epidermal sheet of cells. (C) Quantitation of time of closure, beginning when maximum width of the dorsal opening was 60 μm. D. Quantitation of the rate of zippering. At t = 0, the position of the anterior canthus was noted, and Δd was calculated as the distance in microns from this position to the position of the anterior canthus at the time indicated. (E, F) Close-ups of leading edge in wild-type (E) and mutant (F) embryos. Arrows indicate wavy leading edge.

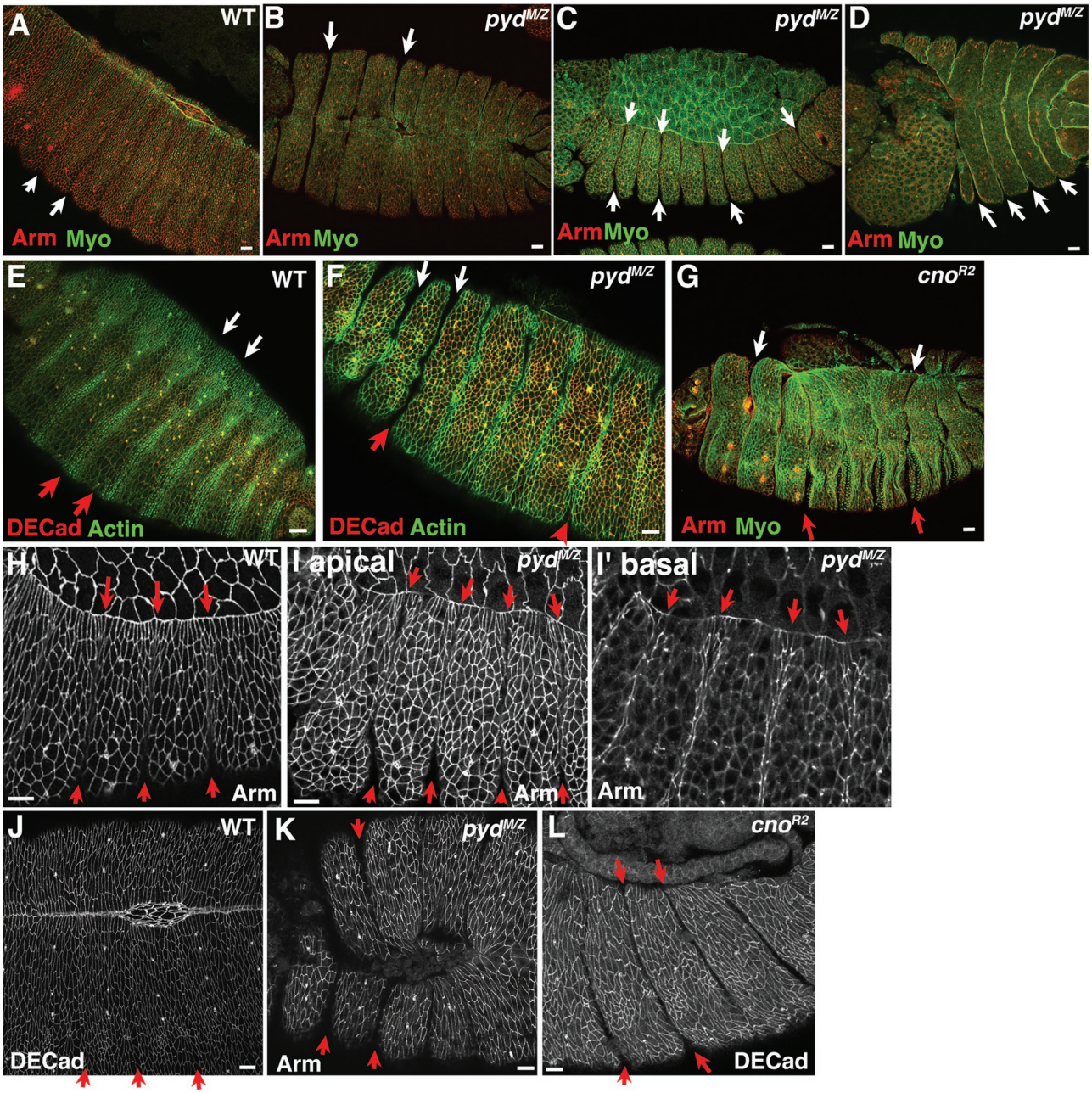

FIGURE 6: Both *pyd*^{MZ} mutants and *cno* zygotic null mutants have persistent segmental grooves that can become extremely deep. Stage 13–15 wild-type (WT), *pyd*^{MZ} mutants, or *cno* zygotic null mutants, anterior left, dorsal up, genotypes and antigens indicated. (A, B) Stage 15. In wild-type embryos (A), segmental grooves have retracted dorsally and are shallow ventrally (arrows). In *pyd*^{MZ} mutants (B), extremely deep segmental grooves remain (arrows). (C) Lateral view, early stage 13. In *pyd*^{MZ} mutants, grooves are already deep at the onset of dorsal closure. (D) Terminal phenotype of severe *pyd*^{MZ} mutant in which dorsal closure and head involution failed—note the continuing presence of deep grooves. (E–G) Ventral (E, F) or lateral views of embryos at stage 15, in which actin-based denticles are forming. In wild-type embryo (E) grooves have completely disappeared ventrally (red arrows) and dorsally (white arrows). In the *pyd*^{MZ} (F) and *cno*^{R2} zygotic mutants (G), extremely deep segmental grooves remain dorsally (white arrows) and ventrally (red arrows), cutting into the developing denticle bands. (H, I) Close-ups, early stage 13. In wild-type embryo, grooves have retracted from the leading edge by two to three cell diameters (H, top arrows) and remain present ventrally (H, bottom arrows). In *pyd*^{MZ} mutants they extend to within one cell of the leading edge (I, top arrows) and are deeper ventrally (I, bottom arrows). I′ basal shows a more basal section, in which the overly deep grooves can be seen in cross section. (J–L) Close-ups, late stage 14. Deep grooves remain in *pyd*^{MZ} (K) and *cno*^{R2} (L) zygotic mutants. Scale bars, 10 μm.

function as a combined pulmonary and vascular system to deliver oxygen to target tissues (reviewed in Ghabrial *et al.*, 2003; Affolter and Caussinus, 2008; Schottenfeld *et al.*, 2010). During embryogenesis, the tracheal system undergoes extensive cell junction rearrangement and shape changes as epithelial cells transform from planar placodes to a ramifying tubular network. Earlier characterization of *pyd* revealed that existing mutations had little effect on the larger tracheal branches but had partially penetrant defects in the

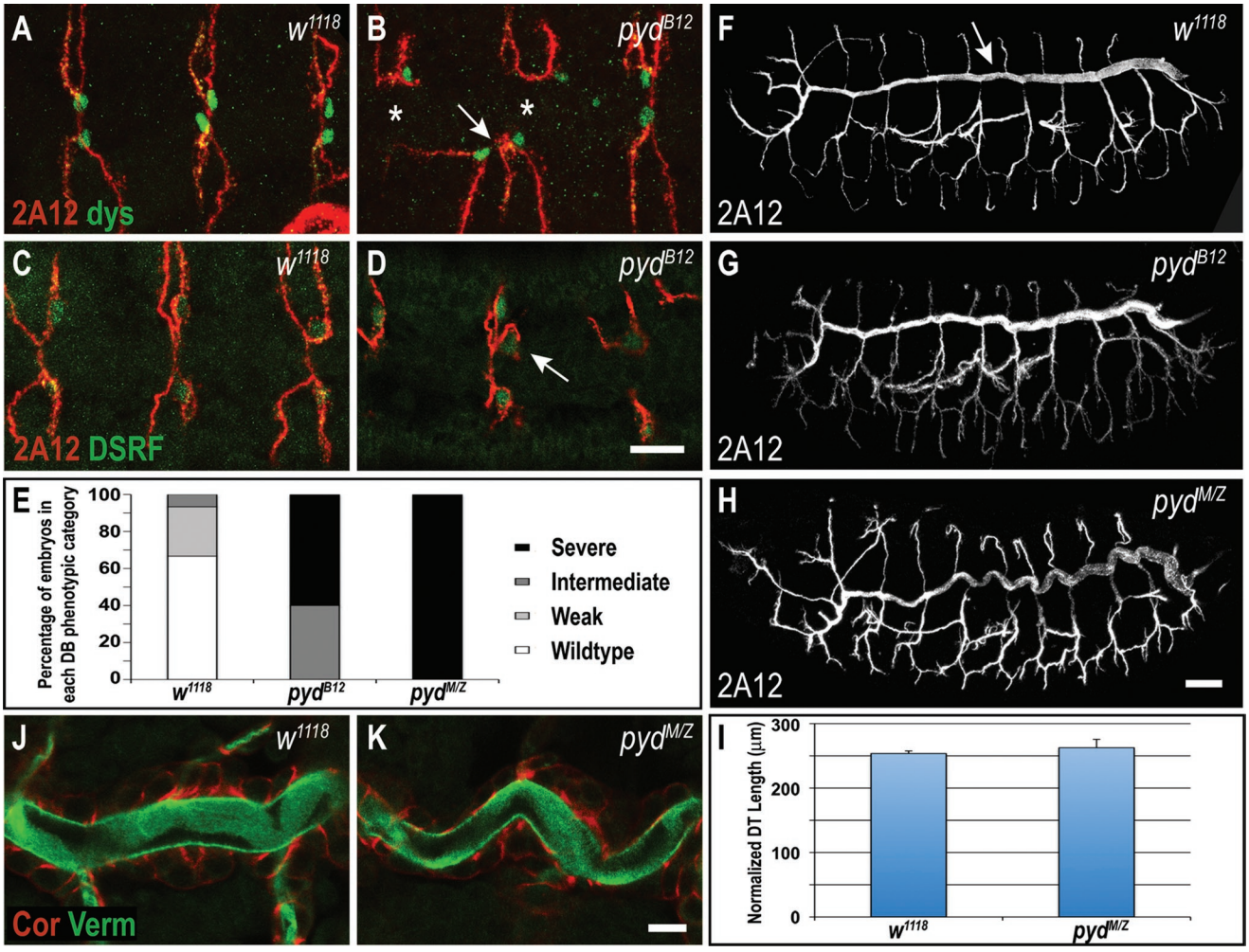

FIGURE 7: Pyd is required for tracheal dorsal branch fusion and cell fate specification but not for formation or maintenance of adherens junctions. (A, B) Many dorsal branches (DBs) in zygotic *pyd*^{B12} mutants fail to fuse (join to contralateral branch, asterisks in B), and often incorrectly fuse to neighboring branches (arrow in B). Anti-Dysfusion (Dys; green) labels fusion cells. (C, D) Labeling for the terminal cell marker DSRF reveals that some DBs in *pyd*^{B12} embryos have more than one terminal cell (arrow in D), whereas control *w*^{1118} embryos have only one terminal cell per DB (C). (E) Quantification of DB defects in zygotic and maternal/zygotic (M/Z) *pyd*^{B12} mutant embryos. DB fusion phenotypes are categorized into four classes as in Jung *et al.* (2006): wild type (complete dorsal branch fusion), weak (only one affected metamere), intermediate (two to four affected metameres), and severe (five or more affected metameres). (F–I) Dorsal trunks (DTs, arrow in F) of zygotic and M/Z *pyd*^{B12} mutants are contiguous, indicating normal adherens junction function and fusion of dorsal trunk segments. (H–I) DTs of *pyd*^{MZ} embryos appear tortuous but are the same length as *w*^{1118} control embryos (p = 0.20, Student's *t* test). DT length is normalized to embryo length. (J, K) *pyd*^{MZ} mutants have normal localization of the septate junction marker Coracle (Cor) and normal lumenal accumulation of the matrix marker Verm. Scale bars, A–D, 5 µm; F–H, 20 µm; J, K, 10 µm.

smaller dorsal branches (DBs) (Jung *et al.*, 2006). To determine whether the comparatively mild phenotypes resulted from the nonnull nature of the tested *pyd* alleles, we examined trachea in *pyd*^{B12} mutant embryos. Zygotic *pyd*^{B12} embryos exhibited defects similar to those of zygotic *pyd*^{C5} and *pyd*^{BG02748} embryos, with DB fusion failures (Figure 7B, asterisks) and ectopic fusions between neighboring DBs (Figure 7B, arrow). Labeling for the terminal cell marker DSRF (*Drosophila* serum response factor) revealed that some DBs in *pyd*^{B12} embryos had more than one terminal cell (Figure 7D, arrow), whereas control *w*^{1118} embryos have only one terminal cell per DB, suggesting that Pyd helps regulate cell fate determination in the DB. Consistent with *pyd*^{B12} being a stronger allele than *pyd*^{C5} and *pyd*^{BG02748}, 60% of zygotic *pyd*^{B12} mutants have severe fusion defects (five or more DBs that fail to fuse; Figure 7E), whereas previous studies reported that <40% of zygotic *pyd*^{C5} and *pyd*^{BG02748} embryos have severe fusion defects (Jung *et al.*, 2006). Elimination of maternal Pyd further increased the frequency and severity of dorsal branch defects, with 100% of *pyd*^{MZ} mutant embryos having severe DB defects (Figure 7E). Thus Pyd has an even more important role in DB morphogenesis than was previously revealed in embryos zygotically homozygous for nonnull alleles (Jung *et al.*, 2006).

To determine whether eliminating Pyd affected other tracheal branches, we examined dorsal trunks (DTs) of zygotic and maternal/zygotic *pyd*^{B12} embryos. AJ proteins are essential for fusion of the segmental sections of the DT into a single tube (Oda and Tsukita, 1999; Beitel and Krasnow, 2000; Cela and Llimargas, 2006). In contrast, Pyd is not essential for fusion, as both zygotic *pyd*^{B12} embryos (Figure 7, F vs. G) and embryos lacking maternal and zygotic *pyd* (Figure 7H) had continuous DTs, without DT discontinuities that would be indicative of AJ defects. This suggests that, as we observed

in the epidermis, Pyd is not essential for AJ assembly or maintenance in trachea.

However, *pyd*^{MZ} mutants did have unexpectedly tortuous trachea (Figure 7H). This phenotype is reminiscent of that present in SJ mutants, which have overelongated tracheal tubes resulting from a failure to secrete the putative chitin-modifying enzyme Vermiform (Verm) into the tracheal lumen (Wang *et al.*, 2006; Paul *et al.*, 2007; Wu *et al.*, 2007; Nelson *et al.*, 2010; Tiklova *et al.*, 2010). Given that three *Drosophila* claudins are critical septate junction components required for Verm secretion (Behr *et al.*, 2003; Wu *et al.*, 2004; Nelson *et al.*, 2010) and that mammalian ZO family proteins are required for apically restricting claudins (Umeda *et al.*, 2006), we tested whether the convoluted tracheal phenotype in *pyd*^{MZ} embryos was due to defects in SJ assembly or function. Labeling for the SJ marker Coracle (Fehon *et al.*, 1994) revealed that the subcellular localization of SJs was normal in *pyd*^{MZ} epithelia (Figure 7K and unpublished data). Lumenal accumulation of Verm was also normal in *pyd*^{MZ} embryos (Figure 7K), suggesting that the organization and function of SJs are not affected by loss of *pyd*. Moreover, careful measurements of the DT using confocal projections demonstrated that, unlike claudin and other SJ mutants, trachea of *pyd*^{MZ} embryos are not significantly longer than those of WT controls (Figure 7I). Thus SJ and claudin defects do not account for the convoluted DTs in *pyd*^{MZ} embryos. Instead, as we recently found for embryos lacking maternal and zygotic Echinoid (Laplante *et al.*, 2010), the tortuous appearance of the DTs most likely results from head involution defects coupled with deep segmental grooves that deflect tracheal tubes without affecting their length. Together, these observations show that Pyd plays a role in normal cell fate specification in the tracheal system and provide further evidence that Pyd is not an essential core component of *Drosophila* adherens or septate junctions.

cno zygotic mutants share many defects with *pyd*^{MZ} mutants

Cno and its mammalian homologue afadin bind fly Pyd and mammalian ZO-1, respectively, and *cno* genetically interacts with *pyd* during embryonic and adult morphogenesis (Takahashi *et al.*, 1998). Previous work documented a role for Cno in dorsal closure and head involution (Miyamoto *et al.*, 1995; Takahashi *et al.*, 1998; Boettner *et al.*, 2003). During dorsal closure, loss of zygotic Cno led to reduced JNK activation in the leading edge, reduced expression of the BMP homologue Dpp by those cells, and failure of cells to properly elongate, leading to ultimate separation of the epidermis and amnioserosa. Reduction of zygotic Pyd enhanced dorsal closure defects of zygotic *cno* mutants, consistent with the idea that they work together in this process (Takahashi *et al.*, 1998).

We thus compared effects of Cno reduction on dorsal closure with that of loss of Pyd. *cno*^{R2} zygotic null mutants (henceforth called *cno* mutants, for simplicity) have a high frequency of defects in head involution and a lower frequency of defects in completing dorsal closure (Sawyer *et al.*, 2009). We first examined how rapidly maternally contributed Cno disappeared in zygotic null mutants. Mutants began to be distinguishable from heterozygous siblings at stage 13 (Figure 8, A′ vs. B′), and zygotic null mutants retain reduced though detectable levels of Cno protein through the end of dorsal closure (Figure 8, C′ vs. D′).

We next compared dynamics of cell shape change in *cno* and *pyd*^{MZ} mutants. We found striking similarities between *pyd*^{MZ} and *cno* mutants. *cno* mutant embryos look largely or completely normal through the onset of dorsal closure (Figure 9, A vs. B). AJs were maintained throughout, with no substantial differences in accumulation of DE-cad (Figure 8, E′ vs. F′) or Arm (Figure 8, G′ vs. H′). Furthermore, at the onset of dorsal closure, both LE cells (Figure 9, I–L, green arrows) and more ventral epidermal cells were able to elongate (Figure 9, K–N, red arrows). *cno* mutant embryos could assemble a leading edge actin (Figure 8, E″ vs. F″) and myosin (Figure 9, G″ vs. H″) cable. In some cells this remained relatively intact through the end of closure. However, in most *cno* mutants, as in *pyd*^{MZ} mutants, the actin cable became uneven as LE cell shapes became nonuniform, with the cable reduced or lost in cells with splayed, open leading edges (Figure 8I, arrows). *cno* mutant LE cells, like wild-type LE cells, also accumulated elevated levels of the nonconventional myosin, myosin VI, both in the cytoplasm and at the leading edge (Figure 8, J vs. K), confirming that *cno* mutant LE cells adopted roughly appropriate fates. Finally, Pyd localization to AJs was unaltered (Figure 8, L vs. M), similar to what we previously observed during early embryogenesis in maternal and zygotic *cno* mutants (Sawyer *et al.*, 2009).

Despite the ability to undergo some of the orchestrated shape changes seen in wild-type embryos, *cno* mutants shared with *pyd*^{MZ} mutants a set of characteristic defects in dorsal closure, with the defects in *cno* more severe in degree. The leading edge of the epidermis in *cno* mutants was wavy rather than straight (Figure 9, C–N; compare wild-type and mutant embryos). LE cells in *cno* mutants were very uneven in shape; some cells had hyperconstricted leading edges (e.g., Figure 9, J, L, and N, white arrows), whereas in other cells the leading edge was broadened (Figure 9, J, L, and N, blue arrows). Zipping together of the two epidermal sheets at the canthi was also significantly slowed, and thus the dorsal opening was oval rather than eye shaped (Figure 9, C–P, yellow arrows in wild-type and mutant embryos). Many mutant embryos failed to close before the onset of muscle contractions and amnioserosal apoptosis; this led to ripping of the amnioserosa (Figure 9P, white arrow), and ultimately some embryos were left totally open dorsally (Figure 9Q, asterisk). In those that did close, cell shapes remained abnormal and small holes sometimes remained (Figure 9, R vs. S). In addition to these alterations in dorsal closure, loss of Cno also mirrored the effects of loss of Pyd on segmental grooves. Segmental grooves in *cno* mutants remain exceptionally deep even after closure should be finished, both dorsally and ventrally (Figure 6, G and L). Thus Cno and Pyd are required for similar aspects of dorsal closure—both play important roles in maintaining LE cell shape, likely through maintaining the attachment or integrity of the actin cable. Both also play roles in epidermal zippering and segmental groove retraction.

Pyd and Cno may act through regulating Ena localization

Given that both loss of Pyd and reduction of Cno lead to similar defects in cell shape change and morphogenesis, we further explored the mechanism by which they act. The suite of defects shared by *pyd*^{MZ} and *cno* mutants was reminiscent of that we previously observed in embryos in which the actin regulator Ena was inactivated (Figure 10, A–C) (Gates *et al.*, 2007). *ena*^{23} maternal/zygotic mutant embryos share with *pyd*^{MZ} and *cno* mutants a wavy leading edge (Figure 10, A and C, red arrows), very similar defects in LE cell shape (Figure 10C, arrows), a reduced rate of zippering of the two sheets together (Gates *et al.*, 2007), and, strikingly, deep and persistent segmental grooves (Figure 10B, arrowheads). Furthermore, segmental groove cells normally have elevated and planar polarized Ena (Gates *et al.*, 2007). We thus considered the hypothesis that Pyd and Cno might act via Ena.

Ena has a complex and interesting localization during dorsal closure (Gates *et al.*, 2007). It localizes to AJs of all epidermal and amnioserosal cells, with particular enrichment at epidermal tricellular

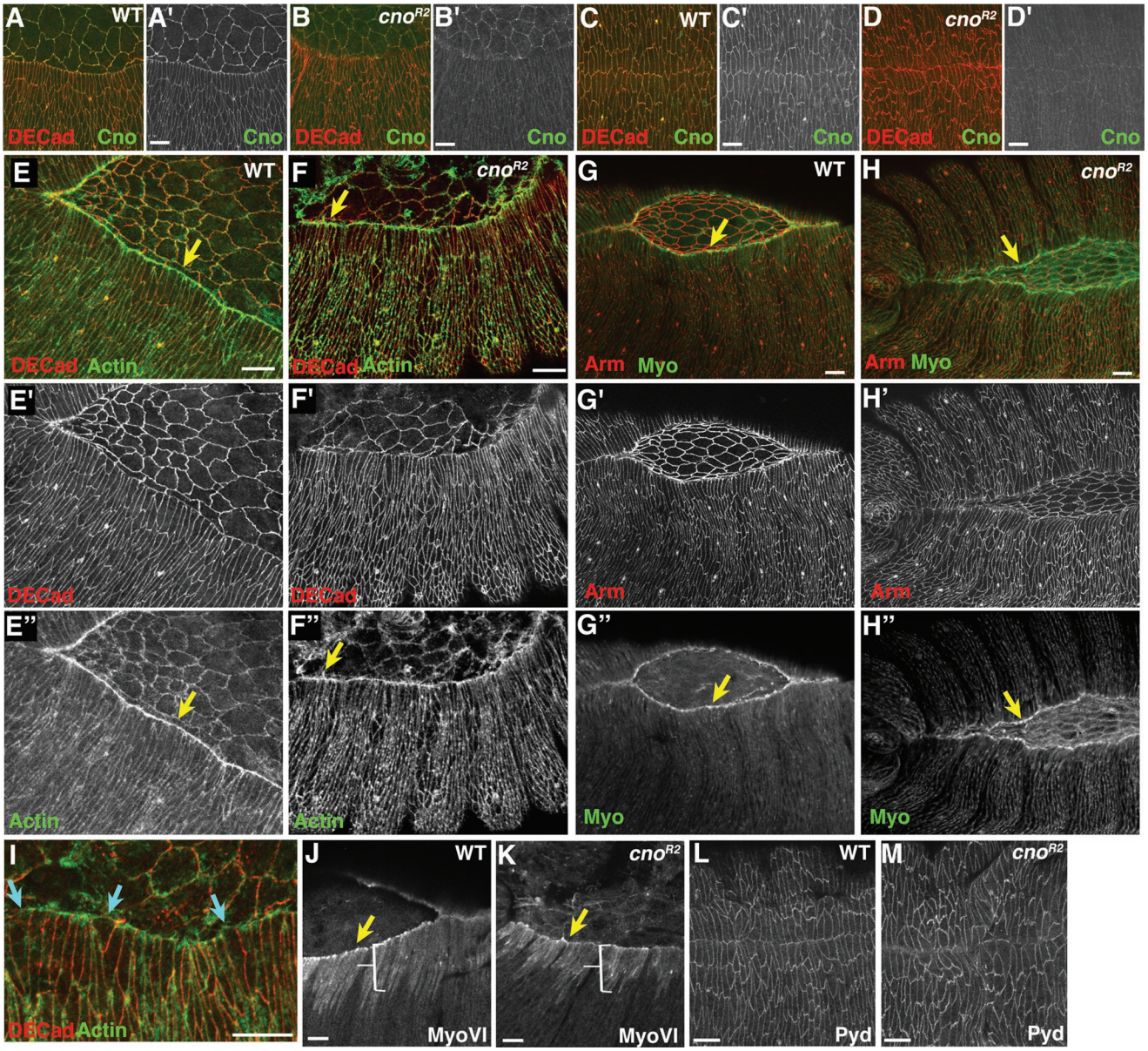

FIGURE 8: *cno* zygotic null mutants can assemble a leading edge actomyosin cable but it is discontinuous in many embryos. Stage 13–15 wild-type (WT) embryo or cno^{R2} zygotic mutants, anterior left, dorsal up, antigens indicated. (A, B) Stage 13. Cno protein levels start to decline in *cno* zygotic mutants (B; imaged on same slide and settings as heterozygous sibling control in A). (C, D) Stage 15. Cno substantially reduced but still detectable in *cno* mutants (D). (E, F) Early stage 14. Actin and DE-cad staining, labeled top to bottom. Arrow, leading edge actin cable. (G, H). Late stage 14. Arm and nonmuscle myosin II (Myo) staining, labeled top to bottom. Arrow, leading edge myosin cable. (I) Late stage 14. In some mutants, the actin cable becomes discontinuous; it is reduced or lost in cells with widened leading edges. (J, K) Late stage 14. Like wild-type embryos, *cno* mutants accumulate elevated levels of myosin VI in the cytoplasm of LE cells (brackets) and particularly at the leading edge (arrows). (L, M) Stage 15. Pyd levels and localization are unaltered in *cno* mutants. Scale bars, 10 μm.

junctions, where three cells meet. However, the most striking localization is to "LE dots," which are at the dorsal ends of cell junctions joining LE cells, where they overlay the amnioserosa. In living embryos, we also observed Ena at the tips of filopodia extended by LE cells. We previously hypothesized that LE dots may serve both to anchor the actin cable at LE cell junctions and serve as storage depots for Ena to be released to regulate LE cell protrusions (Gates *et al.*, 2007; Homem and Peifer, 2009).

We thus explored whether Pyd or Cno is required for proper Ena localization (pyd^{MZ} mutants were stained in parallel with wild-type embryos, and imaged using the same laser settings, to allow accurate comparison of Ena localization and levels in wild-type and mutant embryos). In pyd^{MZ} mutants, Ena was still recruited to tricellular junctions of epidermal cells (Figure 10, H and I, white arrows) and AJs of amnioserosal cells (Figure 10, D′ and E′, red arrows), was still enriched in segmental groove cells (Figure 10, H and I, red arrows), and could still be recruited to LE dots (Figure 10, H and I, blue arrows). However, as dorsal closure proceeded, Ena localization to LE dots was reduced and became quite uneven (Figure 10, D vs. E, arrows, and F vs. G, arrows). In some mid-late dorsal closure embryos, enrichment in LE

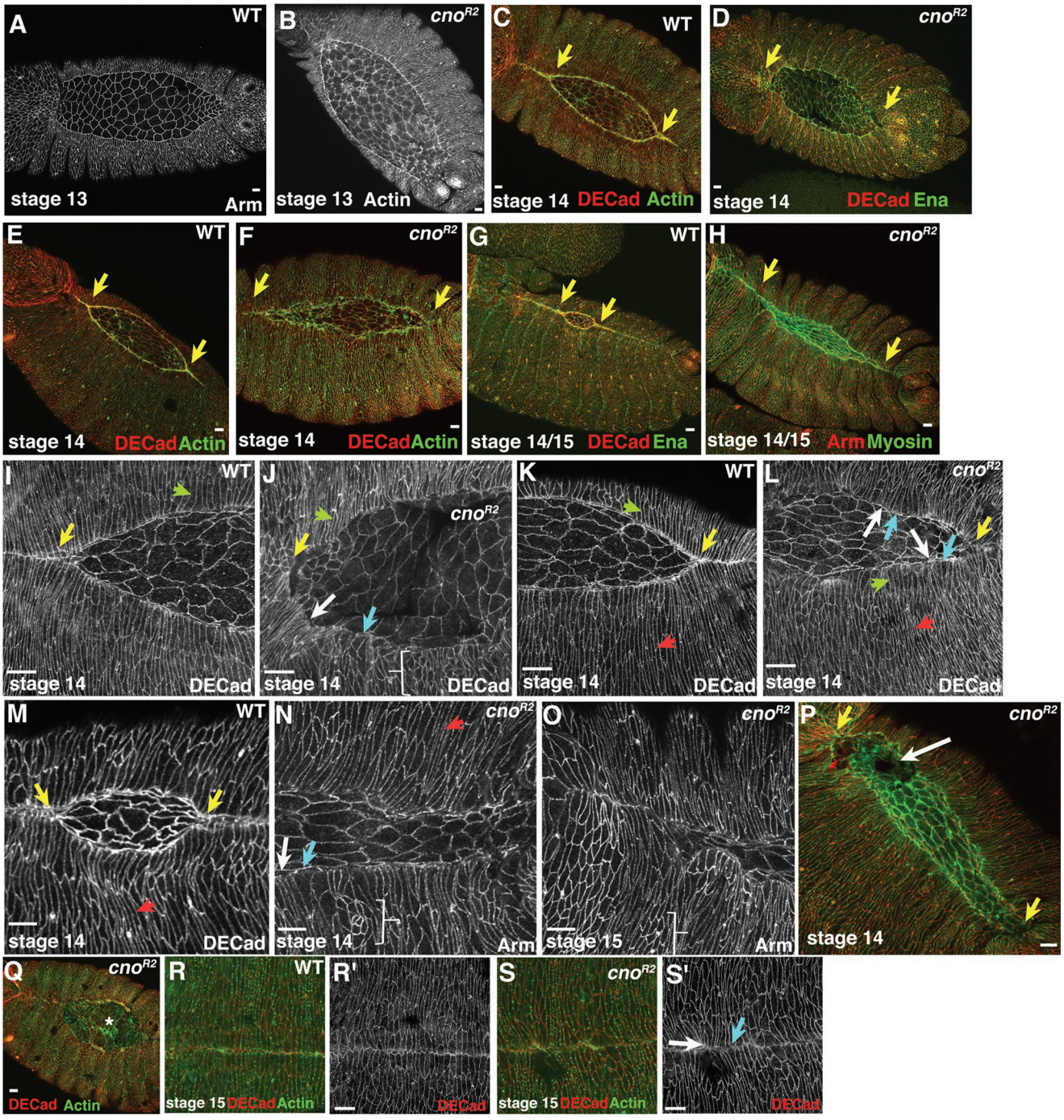

FIGURE 9: *cno* zygotic null mutants have defects in dorsal closure and cell shape change that are very similar to those of pyd^{MZ} mutants. Stage 13–15 wild-type (WT) embryos or cno^{R2} zygotic mutants, anterior left, dorsal view, antigens, genotypes and stages indicated. (A, B) Onset of dorsal closure. *cno* mutants appear quite normal. (C–F) Early stage 14. *cno* mutants have an uneven leading edge and reduced zippering at the canthi (yellow arrows). (G, H) Those defects continue as closure moves to completion. Note the extreme retardation of zippering at canthi in mutants (yellow arrows). (I–O) Close-ups, stage 13 (I, J), early stage 14 (K, L), or late stage 14 (M–O) embryos. Whereas LE cells (green arrows) and more lateral epidermal cells (red arrows) can elongate, substantial defects are seen in cell shape. LE cells often have broadened (blue arrows) or hyperconstricted (white arrows) leading edges, some cells fail to change shape (brackets), and the leading edge of the epidermal sheets is very wavy. (P, Q) In some embryos, the amnioserosa ruptures before completion of dorsal closure (P, white arrow; Q, asterisk). Yellow arrows indicate retarded zippering. (R, S) stage 15. In the subset of mutants completing closure, cell shapes remain irregular (blue arrow) and small dorsal discontinuities are seen (white arrow). Scale bars, 10 μm.

dots was almost lost (Figure 10, L vs. M, arrows, and N vs. O, arrows), whereas in others it was substantially reduced (Figure 10, K and Q, arrows). We also examined Ena localization in *cno* zygotic mutants, using heterozygous wild-type siblings as internal controls. We observed very similar irregularities in Ena localization to LE dots in *cno* mutants (Figure 10, R vs. S, arrows, and T vs. U, arrows).

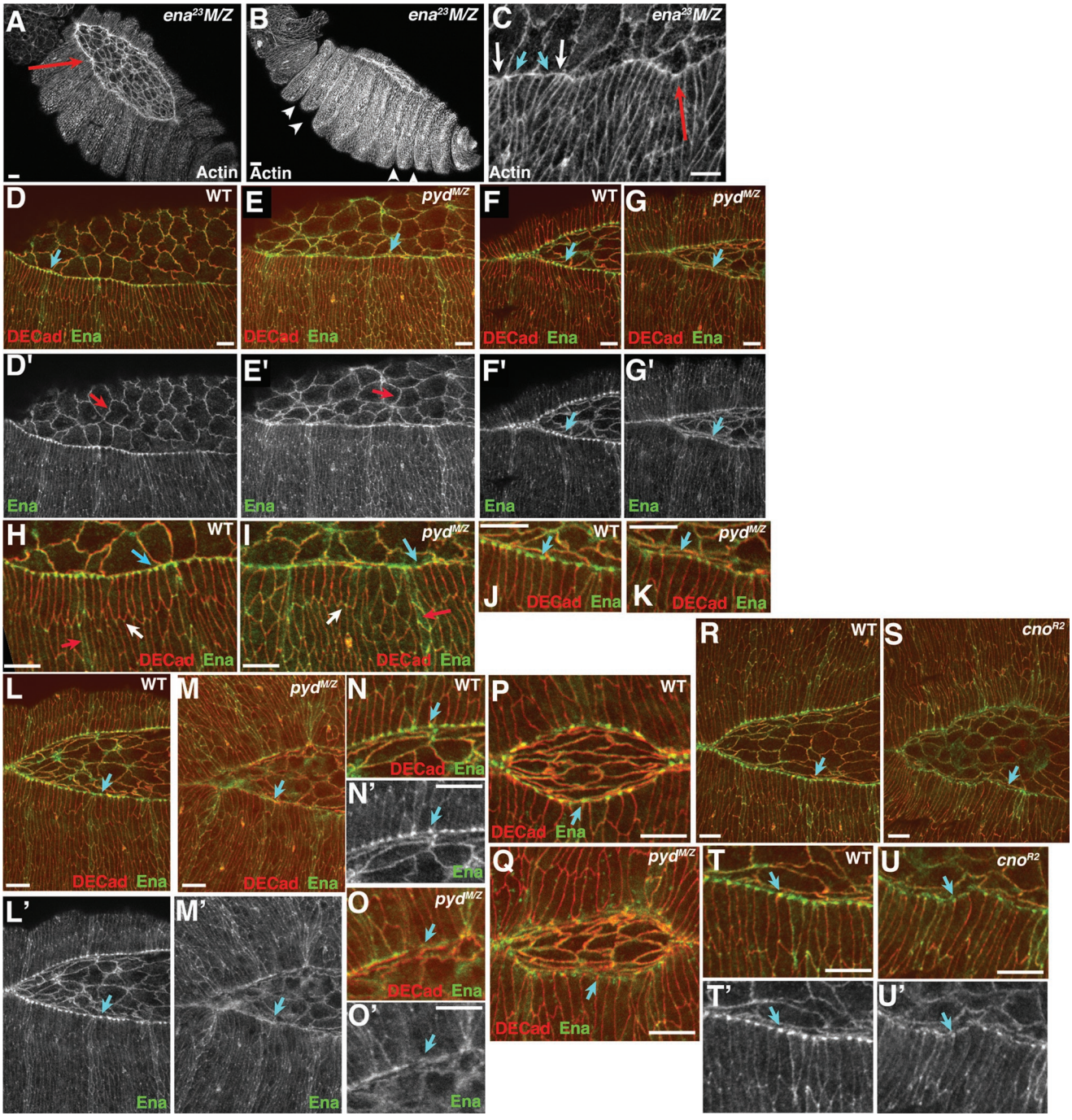

FIGURE 10: Loss of Pyd or reduction of Cno disrupts Ena localization to LE dots and mimics Ena loss of function. (A–C) *ena*^{23} maternal/zygotic mutants. Note the wavy leading edge (A, arrow), very deep segmental grooves (B, arrowheads), and uneven cell shapes of LE cells, with hyperconstricted (C, white arrows) and splayed open (C, blue arrows) leading edges. (D–P) *pyd*^{MZ} and control wild-type embryos stained and imaged in parallel to visualize DE-cad and Ena. (H, I) Close-ups of D, E. (J, K) Close-ups of F, G. (N, O) Close-ups of L, M. (D, E, H, I) Early stage 14. Blue arrows indicate LE dots. Red arrows in D′ and E′ indicate amnioserosal cell junctions. Red arrows in H and I indicate Ena enrichment in segmental groove cells. White arrows indicate Ena in tricellular junctions. (F, G, J–Q) Late stage 14. Arrows indicate LE dots. In *pyd*^{MZ} mutants, the amount of Ena in LE dots is reduced (F, G, J, K, P, Q) or almost eliminated (L–O). (R–U) *cno*^{R2} mutants and heterozygous wild-type siblings visualized identically. In *cno*^{R2} mutants, Ena in LE dots is strongly reduced (S and U, arrows). Scale bars, 10 μm.

These data suggested that Pyd and Cno might act through Ena. To further test this hypothesis, we looked for genetic interactions between *ena* and *cno*, using embryonic cuticles to assess effects on morphogenesis. *ena*^{23} zygotic mutants have little effect on the epidermis—90% of mutants have virtually wild-type cuticles, whereas 8% have head holes (Gertler *et al.*, 1990; Gates *et al.*, 2007; Figure 11) (*ena* embryonic lethality is thought to be due to defects in axon guidance). In contrast, 84% of *cno*^{R2} zygotic null mutants have defects in head involution ranging from mild to severe defects in the head skeleton hole, whereas 16% have a head or dorsal

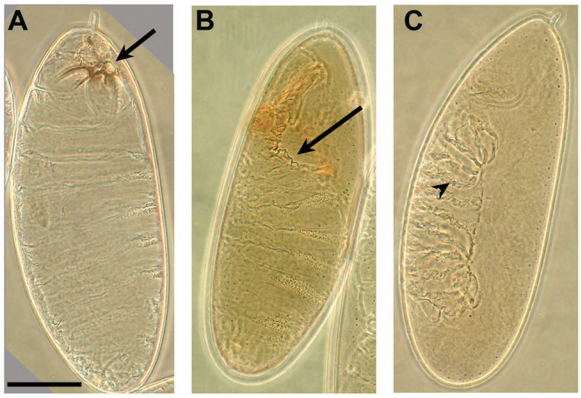

D

Female x male		Mild to severe head defects	Head or dorsal hole	Only ventral cuticle remaining		Embryonic lethality
cno^{R2}/+ x cno^{R2}/+	=*cno* zygotic	84%	16%	0%	n=95	23% lethal (25% expected)
ena^{23}/+; cno^{R2}/+ x cno^{R2}/+	=*cno* zygotic + Ena reduced	58%	38%	4%	n=159	37% lethal (25% expected)
ena^{23}/+ x ena^{23}/+	=*ena* zygotic	90%	8%	0%	n=332	19% lethal (25% expected)
ena^{23}/+; cno^{R2}/+ x ena^{23}/+	=*ena* zygotic + Cno reduced	50%	50%	0%	n=104	25% lethal (25% expected)
ena^{23}/+; cno^{R2}/+ x ena^{23}/+; cno^{R2}/+	genotypes include double mutants Cno reduced	57%	33%	10%	n=202	41% lethal (44% expected)

FIGURE 11: *cno* and *ena* exhibit strong, dose-sensitive genetic interactions. (A–C) Cuticles of embryos, exhibiting representative phenotypes scored in the different genotypes. (A) Example of mild to severe defects in the head skeleton (arrow), indicative of defects in head involution. (B) Example of the more severe phenotypic class, exhibiting either a head hole due to complete failure of head involution (arrow; illustrated here), a large dorsal hole, indicating failure of dorsal closure (not shown), or both. (C) Example of novel phenotypic class only seen in genetic interaction experiments, in which only the ventral cuticle (identified by the presence of denticle belts; arrowhead) remained. (D) Percentages of dead embryos in each phenotypic class for different genetic interaction crosses. Column at far right indicates embryonic lethality—expected percentages assume that only embryos homozygous for *cno, ena*, or both die. Scale bar, 75 µm.

cuticle hole, indicating failure of head involution and/or dorsal closure (Figure 11) (Sawyer *et al.*, 2009). Simply reducing maternal and zygotic Ena levels enhanced the *cno* zygotic phenotype (cno^{R2}/+;ena^{23}/+ × cno^{R2}/+; mothers and some embryos thus heterozygous for *ena*)—now 38% of the progeny had head and/or dorsal holes, and 4% had a novel, stronger phenotype in which only ventral cuticle remained (Figure 11). Reducing maternal and zygotic Cno levels (cno^{R2}/+;ena^{23}/+ × ena^{23}/+; mothers and some embryos thus heterozygous for *cno*) also strongly enhanced the *ena* zygotic phenotype—now 50% of the progeny had head holes, consistent with all *ena* mutant embryos that were maternally and zygotically *cno*/+ having this phenotype (Figure 11). When we crossed females and males heterozygous for both *cno* and *ena*, thus generating both double mutants and single mutants with a reduced maternal dose of the other gene, we saw even more striking enhancement of the *cno* phenotype (lethal embryos are a 2:2:1 mix of *ena* mutants, *cno* mutants, and *ena;cno* double mutants), with 10% of the total lethal mutants and thus likely about half of the double mutants now having only ventral cuticle remaining (Figure 11). These results are consistent with essentially all double mutants having completely failed in dorsal closure. Thus *ena* and *cno* exhibit strong, dose-sensitive genetic interactions.

We next explored whether *ena* genetically interacts with *pyd*. As we observed with Cno, reducing Pyd levels (by crossing *ena*/+;*pyd*/+ males and females) strongly enhanced the morphogenesis defects of *zygotic ena* mutants, substantially increasing the frequency of failure of head involution (Figure 12F, bottom four genotypes). This was true for two different *pyd* alleles, pyd^{B12} *and* pyd^{ex180}. In addition, reducing Ena levels also substantially enhanced the severity of the pyd^{MZ} phenotype; more than one-third of the mutants now exhibited large holes in the cuticle, suggesting disruption of epithelial integrity (Figure 12F, top two genotypes). The dose-sensitive genetic interactions of *ena* with both *cno* and *pyd* are consistent with those seen with joint reduction of proteins in the same pathway and support the hypothesis that Cno and Pyd work with or through Ena during embryonic morphogenesis.

DISCUSSION

Cell biological studies in cultured cells suggest that mammalian ZO family proteins play important roles in assembly of mammalian TJs and also play important roles in the maturation of AJs in vitro (Fanning and Anderson, 2009). These data suggest that they may also play key roles in regulating epithelial architecture, morphogenesis, and barrier function during normal development and organogenesis. This hypothesis is further supported by genetic studies in mice, nematodes, and flies, but genetic redundancy in mammals and the absence of clear null alleles in *Drosophila* have thus far precluded completely eliminating function of the ZO family and

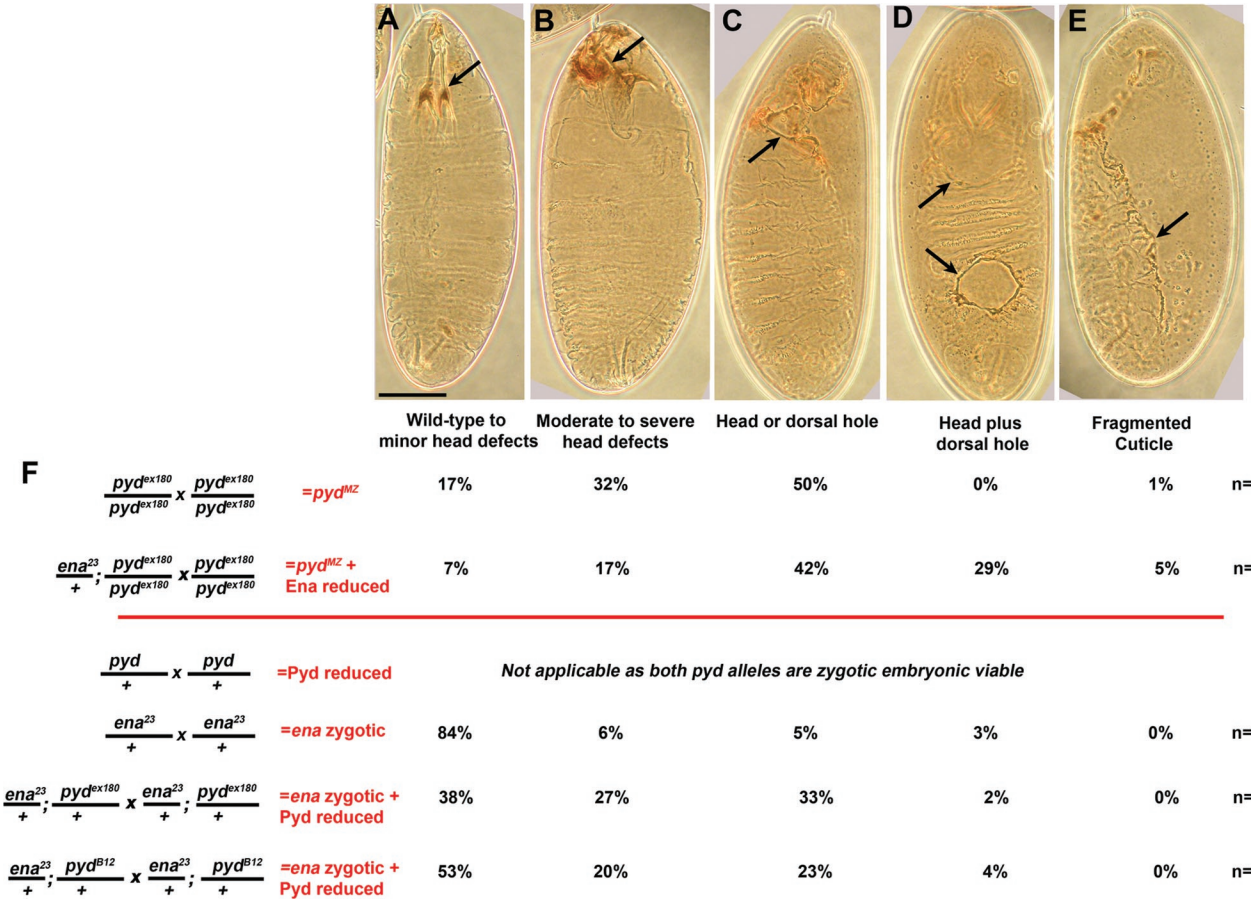

FIGURE 12: *pyd* and *ena* also exhibit strong, dose-sensitive genetic interactions. (A–E) Cuticles of embryos, exhibiting representative phenotypes scored in the different genotypes. (A) Example of normal or nearly normal head skeleton (arrow). (B) Example of moderate to severe defects in the head skeleton (arrow), indicative of defects in head involution. (C) Example of a more severe phenotypic class, exhibiting either a head hole due to complete failure of head involution (arrow; illustrated here), a large dorsal hole, indicating failure of dorsal closure (not shown), or both. (D) Example of an embryo in which head involution failed (top arrow) and there was one or more holes in the dorsal cuticle (bottom arrow). (E) Example of the most severe phenotype, in which the remaining cuticle was fragmented. (F) Percentages of dead embryos in each phenotypic class for different genetic interaction crosses. Note that this actually underestimates the enhancement of the *ena* phenotype by reduction of Pyd levels, as not all *ena* zygotic mutant embryos die (19% relative to 25% expected from the cross), whereas essentially all *ena* zygotic mutants with reduced Pyd die (25% relative to 25% expected). Presumably those *ena* zygotic mutants that hatch as larvae have an essentially wild-type cuticle phenotype. Scale bar, 75 μm.

assessing its roles in the development of these two model animals. Our new null allele of the single fly ZO family protein Pyd allowed us to carry out this analysis.

Pyd is not essential for junctional assembly or maturation

ZO family proteins localize to mammalian TJs and also to AJs in mammals, flies, and nematodes (Fanning and Anderson, 2009). Elegant work in cell culture revealed important roles for mammalian ZO family proteins in properly localizing TJ strands into a functional, apically-localized barrier (Umeda *et al.*, 2006). Furthermore, whereas cultured mammalian cells lacking ZO family function can assemble AJs, their maturation into smooth belt junctions, a phenotype thought to involve remodeling the linkage to the actin cytoskeleton, is impaired (Ikenouchi *et al.*, 2007).

We thus hypothesized that ZO family proteins would be essential for AJ maturation and/or maintenance during normal development. However, assembly of spot AJs into more continuous belt AJs occurred normally in pyd^{MZ} mutants, and there were no apparent defects in DE-cad levels or localization, even late in embryonic morphogenesis. Furthermore, loss of Pyd did not perturb tracheal trunk fusion, an event that requires AJ function. Finally, loss of Pyd did not perturb the junctional localization of its AJ binding partner Cno. Our data also suggest that Pyd is dispensable for assembly of tracheal septate junctions—although this is perhaps not surprising, as fly Pyd does not localize to septate junctions. Our data are consistent with analysis of the nematode ZO-1 orthologue ZOO-1 (Lockwood *et al.*, 2008), which is also dispensable for AJ assembly. It will be interesting to examine mouse ZO family double and triple mutants to determine the full role of these proteins in both AJs and TJs during mammalian development.

We cannot rule out subtle changes in levels of AJ proteins in the absence of Pyd. Djiane *et al.* (2011) recently reported that although AJs remain in *pyd* mutant cells, cells lacking Pyd accumulate higher levels of membrane-associated DE-cad than neighboring wild-type cells. Their data provide support for a model in which Pyd binds and may regulate the E3 ubiquitin ligase Su(dx), which regulates the endocytic trafficking of Notch.

Perhaps Pyd plays a similar role in regulating the trafficking of AJ proteins.

We did not explore Pyd's role in Notch signaling during postembryonic development, as that was the subject of parallel work from Sarah Bray and Martin Baron's labs (Djiane *et al.*, 2011). However, our data do not support an essential role for Pyd in embryonic Notch signaling, as *Notch* mutant embryos lose ventral epidermal cells and gain excess neurons, phenotypes we did not observe. We certainly cannot rule out subtler roles for Pyd in Notch or other signaling pathways in the embryo—in fact, the presence of extra terminal cells in the tracheal system may be indicative of Notch signaling defects in that tissue (Llimargas, 1999).

Pyd plays important roles in embryonic cell shape changes and morphogenetic movements

Although Pyd is not essential for assembly or maintenance of AJs, we found that it does play important roles in embryonic morphogenesis in both the epidermis and trachea. From 40 to 70% of embryos lacking maternal and zygotic Pyd die as embryos, with characteristic defects in head involution. This was true in embryos mutant for three different deletion alleles, two of which did not remove any other coding sequences. Even for events that usually go to completion in the absence of Pyd, like dorsal closure, execution does not proceed normally. For example, loss of Pyd disrupts coordinated cell shape changes in the epidermis during dorsal closure and significantly slows this process. Pyd also plays an important role in effective zippering together of the two epidermal sheets at the canthi and in maintaining a straight leading edge. Furthermore, the tracheal defects we observed are consistent with defects in intercalation, as were previously documented in weaker alleles (Jung *et al.*, 2006), along with possible defects in cell fate. Thus fly Pyd, like nematode ZOO-1 (Lockwood *et al.*, 2008), is an important regulator of morphogenesis. Because Pyd is a complex, multidomain protein with many binding partners, in the future, it will be of interest to explore how the different domains of ZO-1 contribute to its functions in vivo.

Of interest, zygotic *cno* mutants share all of the cell shape and morphogenesis defects of pyd^{MZ} mutants. This is consistent with early data demonstrating both physical and genetic interactions (Takahashi *et al.*, 1998), thus strongly suggesting that Cno and Pyd work together in regulating coordination of adhesion and the cytoskeleton. Our recent work suggests that during apical constriction and invagination of mesoderm cells, Cno is one of the linkers anchoring the actomyosin cytoskeleton at AJs (Sawyer *et al.*, 2009). Consistent with this idea, we observed apparent rupture of the LE actomyosin cable in both pyd^{MZ} and *cno* mutants, leading to splayed open and hyperconstricted LE cells. During dorsal closure, our data would be consistent with a model in which Cno and Pyd specifically reinforce AJ–actomyosin connections at points where tension is the greatest. It will be interesting to examine whether mammalian ZO-1/ZO-2 and afadin functionally interact in a similar way.

Another player in dorsal closure is the fly nectin-like protein Echinoid (Ed). Like the mammalian nectins, Ed is an immunoglobulin-superfamily cell adhesion molecule. Both nectins and Ed associate with afadin/Canoe (Takai *et al.*, 2008; Wei *et al.*, 2005). Ed plays an important role during dorsal closure (Lin *et al.*, 2007; LaPlante and Nilson, 2011), and Ed (Laplante *et al.*, 2010), like Pyd, plays a role in tracheal development. During dorsal closure, Ed expression is lost from the amnioserosa but maintained in the epidermis (Lin *et al.*, 2007; Laplante and Nilson, 2011), and juxtaposition of adjacent cells that express and those that do not express Ed can lead to actin cable assembly (Wei *et al.*, 2005; Laplante and Nilson, 2006). However, *ed* maternal and zygotic mutants differ from both pyd^{MZ} and *cno* zygotic mutants, as in *ed* mutants the actomyosin cable fails to assemble. Furthermore, unlike Ed, Cno and Pyd continue to be expressed in the amnioserosa. The mechanistic role of Ed remains somewhat controversial, with suggestions that it works through fly myosin VI to regulate myosin contractility (Lin *et al.*, 2007) and suggestions that it sets up a tissue boundary, allowing proper polarization of junctional and cytoskeletal proteins in the leading edge (Laplante and Nilson, 2011). It will be interesting to explore whether Ed, Cno and Pyd work together during dorsal closure.

Do Pyd and Cno regulate morphogenesis in part through regulating Ena localization?

The suite of defects during dorsal closure shared by pyd^{MZ} and *cno* mutants is complex, including defects in LE cell shapes, a wavy leading edge, defects in zippering at the canthi, persistent deep segmental grooves, and simultaneous disruption of head involution. This entire suite of defects was strikingly reminiscent of those we previously observed in embryos in which the function of the actin regulator Ena was disrupted by genetic inactivation, sequestration to mitochondria, or expression of a constitutively active form of its negative regulator Abelson (Abl) kinase (Gates *et al.*, 2007; Stevens *et al.*, 2007). This led us to explore the hypothesis that Pyd and Cno worked together with or regulated Ena.

During dorsal closure, Ena has an interesting localization pattern in epidermal cells. It localizes to AJs and is particularly enriched at tricellular junctions. It also localizes to ends of filopodia produced by LE cells. However, the most striking feature of Ena localization during this stage is its dramatic accumulation in "LE dots," which form at the dorsal ends of the AJs between LE cells, where they overlay the amnioserosa. These overlap locations where the actomyosin cable is anchored. We initially hypothesized LE dots might play a role in cadherin-based cell adhesion, but this is not disrupted in *ena* mutants (Gates *et al.*, 2007). Reducing Ena function does reduce filopodia, which we suspect underlies defects in zippering of the epidermal sheets (Gates *et al.*, 2007). The role of Ena in LE dots is less clear. We have speculated that LE dots are Ena storage places, from which it is released to modulate cell protrusions at the leading edge. Consistent with this, activation of the formin Diaphanous leads to loss of Ena from LE dots and dramatic alterations in protrusive behavior (Homem and Peifer, 2009). However, the defects seen in LE cell shape in *ena* mutants (Gates *et al.*, 2007) are also consistent with the idea that Ena plays a role in anchoring or maintaining the actin cable at the leading edge.

We saw clear alterations in Ena localization in LE cells in pyd^{MZ} or *cno* mutants. Enrichment of Ena in LE dots was reduced overall and became very uneven. It is tempting to speculate that the failure to effectively recruit Ena to LE dots leads to the defects in LE cell shape we observed in pyd^{MZ} or *cno* mutants. If failure to deliver Ena to LE dots also interfered with subsequent release to the leading edge, this might alter protrusive behavior and slow zippering of the epidermal sheets at the canthi—this remains to be tested. To test the hypothesis that regulating Ena is an important part of the roles of Pyd and Cno during dorsal closure, we examined genetic interactions. Loss of zygotic Ena has only a subtle effect on epidermal morphogenesis (Gertler *et al.*, 1990), as the maternal Ena suffices for most events (Gates *et al.*, 2007). However, reduction of maternal/zygotic Ena significantly enhanced the epidermal phenotype of zygotic *cno* mutants, and reduction of maternal/zygotic Cno enhanced the epidermal phenotype of zygotic *ena* mutants, consistent with

Antibodies/probes	Dilution	Source
Anti–DE-cad2	1:100	Developmental Studies Hybridoma Bank, University of Iowa, Iowa City, IA (DSHB)
Anti-zipper (myosin II heavy chain)	1:1000	D. Kiehart (Duke University, Durham, NC)
Anti-Armadillo (N27A1)	1:100	DSHB
Anti-Cno	1:1000	J. Sawyer and N. Harris (University of North Carolina at Chapel Hill)
Anti-Cor	1:10000	R. Fehon (University of Chicago, Chicago, IL)
Anti-Verm	1:300	S. Lushnig (Universität Zürich, Zürich, Switzerland)
Anti-DSRF	1:500	S. Blair (University of Wisconsin, Madison, WI)
Anti-Dys	1:800	L. Jiang (Oakland University, Rochester Hills, MI)
Monoclonal-2A12	1:500	DSHB
Alexa-phalloidin	1:500	Molecular Probes, Invitrogen, Carlsbad, CA
	Secondary antibodies:	
Alexas 488, 568, and 647	1:500	Molecular Probes, Invitrogen

TABLE 3: Antibodies and probes.

them working together during this process; it is important to note that in both zygotic mutants maternal Ena or Cno remains, so enhancement is a plausible prediction for double mutants of genes in the same pathway. It will be interesting to further explore this mechanistic connection, probing whether Ena physically interacts with either Cno or Pyd and how they regulate Ena localization and/or activity.

MATERIALS AND METHODS

Fly stocks

The stocks *pyd*^{BG02748}, *pyd*^{tam1}, and *Df(3R)p-XT103* and isogenic lines required for FLP-mediated recombination were obtained from the Bloomington Stock Center (Indiana University, Bloomington, IN). *pyd*^{f05901} and *pyd*^{c03468} were from the Exelixis Collection at Harvard Medical School (Boston, MA). *CG8379*$^{5\text{-}HA\text{-}1806}$ was from the Szeged *Drosophila* Stock Centre (Szeged, Hungary; now available from the *Drosophila* Genetic Resource Center, Kyoto, Japan). *pyd*^{C5} was kindly provided by Hillary Ellis and Jennifer Zallen (Memorial Sloan Kettering, New York, NY). Moesin-GFP was a gift from Daniel Kiehart (Duke University, Durham, NC).

Generating *pyd*^{B12}

The *pyd* deficiency allele *pyd*^{B12} was generated by FLP-mediated site-specific recombination between the FRT sites of P[RS5] CG8379$^{5\text{-}HA\text{-}1806}$ and PBac[WH]pyd^{f05901} according to established protocols (Parks *et al.*, 2004; Ryder *et al.*, 2004). All resulting alleles were screened by PCR to establish the presence of the hybrid P-arms, and lines containing the ~37-kb deletion were analyzed by Western blotting with the PYD1 antibody to confirm loss of zygotic Pyd expression. *pyd*-deficient lines were further screened by crossing to themselves or *Df(3R)p-XT103*, a deficiency line with a >550-kb deletion including the *pyd* coding region. We found zygotic lethality in homozygotes that was not present over *Df(3R)p-XT103*. This second-site lethal mutation was eliminated by outcrossing three times to isogenic *w*^{1118}.

Generating anti-Pyd antibody PYD1

The mAb PYD1 was generated by the Immunology Core Facility at the University of North Carolina at Chapel Hill, using a Pyd-derived peptide (NH_2-CNGLNDEKSNLTPRGRSRG; amino acids 327–344 of Pyd-PB) that is found in all potential Pyd isoforms (Figure 1A). Hybridoma culture supernatants were purified on protein G-Sepharose and used at 1:2000 for Western blots and 1:1000 for immunocytochemistry.

Western blots

To analyze Pyd expression in embryos, *pyd*^{B12} homozygous and heterozygous 14- to 18-h embryos were sorted from balanced stocks (*TM3, P{GAL4-twi.G}2.3*, *P{UAS-2xEGFP}AH2.3*, *Sb*^{1} *Ser*^{1}). Thirty embryos were lysed in 30 ml of ice-cold lysis buffer (25 mM HEPES, 100 mM NaCl, 1 M $MgCl_2$, 1 mM $CaCl_2$, and 0.5% Triton X-100, with Complete Mini protease inhibitors [Roche Diagnostics, Indianapolis, IN], pH 7.5), frozen at −20°C overnight and crushed with the blunt end of a paperclip. The lysate was clarified at 100,000 × *g*, and the soluble supernatant was removed with a fine glass needle. This supernatant was mixed with an equal volume of SDS–PAGE sample buffer, and ~6–10 embryo equivalents were resolved by electrophoresis. To analyze Pyd expression in adults, 25 heads (13 female, 12 male) were isolated from sorted stocks and processed as described. Proteins from ~5 heads were resolved by SDS–PAGE and analyzed by Western blotting with PYD1.

Cuticle preparation

Embryos were collected and allowed to develop for 72 h at 25°C. Unhatched embryos were washed in 0.1% Triton X-100 and dechorionated in 50% bleach for 5 min in a nutator. After washing three times in 0.1% Triton, embryos were mounted in 1:1 diluted Hoyer's medium:lactic acid and incubated at 60°C overnight.

Immunofluorescence/live imaging

Dechorionated embryos were fixed in 1:1 4% formaldehyde in phosphate-buffered saline (PBS):heptane or 1:1 3.7% paraformaldehyde in PBS:heptane (tracheal experiments) for 20 min or in hot Triton salt (0.03% Triton X-100 in 68 mM NaCl) for 5 s followed by fast cooling on ice (for myosin heavy chain) and devitellized by vigorous shaking in 1:1 heptane:methanol or by hand peeling using a scalpel (for staining F-actin by phalloidin). After three washes with 0.01% Triton X-100 in PBS (PBS-T), embryos were blocked in 1% normal goat serum (NGS) in PBS-T or 0.5% bovine serum albumin in PBS-T (tracheal experiments) overnight. Primary and secondary antibodies (sources and dilutions are listed in Table 3) in PBS-T/NGS were sequentially incubated and embryos mounted in Aqua-Poly/Mount (Polysciences, Warrington, PA). Digital images were obtained on a confocal laser-scanning microscope (LSM 5 PASCAL; Carl Zeiss, Jena, Germany) or a Leica TCS SP2 (tracheal experiments)] using a 40× objective (Plan-NeoFluar [Carl Zeiss], numerical aperture [NA] 1.3) and processed using LSM 510 AIM software (Carl Zeiss). For live imaging, dechorionated embryos were mounted in halocarbon oil (series 700; Halocarbon Products Corporation, River Edge, NJ) on a gas-permeable membrane (petriPERM 50, hydrophobic; Sartorius, Göttingen, Germany). Time-lapse microscopy was performed using an UltraVIEW spinning disk confocal system (PerkinElmer, Waltham,

MA), ORCA-ER camera (Hamamatsu, Hamamatsu City, Japan), Nikon Plan Apo 40× NA 1.3 or Plan Apo VC 100× NA 1.4 objectives (Nikon Instruments, Melville, NY), and MetaMorph software (Molecular Devices, Sunnyvale, CA). Dorsal closure timing was analyzed by setting the initial DV opening of 60 mm (measured in MetaMorph) for all movies and calculating the time for each opposing leading edges to meet along the entire length. The same movies were used to analyze zippering kinetics by calculating the distance (millimeters) of canthi movement along the anterior–posterior length at each time point and presented as an average value with SD. For statistical analysis, an unpaired *t* test was performed on the DV closing time (Figure 5C) and the slope of zippering rate (Figure 5D) using SigmaPlot software (Systat Software, San Jose, CA). Adobe Photoshop CS2 (Adobe, San Jose, CA) was used to adjust input levels so the main range of signals spanned the entire output grayscale and to adjust brightness and contrast.

ACKNOWLEDGMENTS

We are especially grateful to James Anderson for his support and encouragement in early stages of this work and to Sarah Bray for sharing fly stocks and information before publication. We thank Bradley Bone and the University of North Carolina Immunology Core Facility for production of PYD mAb, Colby Allred for technical assistance, Jennifer Zallen, Dan Kiehart, the Developmental Studies Hybridoma Bank, and the Bloomington Stock Center for reagents, Don McEwen, Swati Bannerjee, Jennifer Zallen, Midori Seppa, Ross Cagan, and our lab members for many thoughtful conversations, Jennifer Holmes and Jacey Bennis for technical assistance, and Julie Gates for the *ena* mutant pictures. This work was supported by National Institutes of Health grant R01GM47957 to M.P., National Institutes of Health grant R01DK061397 to A.S.F. and James Anderson and National Institutes of Health grant R01GM069540 to G.J.B. K.S.N. was supported by National Institutes of Health grant T32 GM008061 and a Malkin Scholar award.

REFERENCES

Adachi M, Inoko A, Hata M, Furuse K, Umeda K, Itoh M, Tsukita S (2006). Normal establishment of epithelial tight junctions in mice and cultured cells lacking expression of ZO-3, a tight-junction MAGUK protein. Mol Cell Biol 26, 9003–9015.

Affolter M, Caussinus E (2008). Tracheal branching morphogenesis in *Drosophila*: new insights into cell behaviour and organ architecture. Development 135, 2055–2064.

Anderson JM, Van Itallie CM (2009). Physiology and function of the tight junction. Cold Spring Harb Perspect Biol 1, a002584.

Behr M, Riedel D, Schuh R (2003). The claudin-like megatrachea is essential in septate junctions for the epithelial barrier function in *Drosophila*. Dev Cell 5, 611–620.

Beitel GJ, Krasnow MA (2000). Genetic control of epithelial tube size in the *Drosophila* tracheal system. Development 127, 3271–3282.

Boettner B, Harjes P, Ishimaru S, Heke M, Fan HQ, Qin Y, Van Aelst L, Gaul U (2003). The AF-6 homolog canoe acts as a Rap1 effector during dorsal closure of the *Drosophila* embryo. Genetics 165, 159–169.

Boettner B, Van Aelst L (2009). Control of cell adhesion dynamics by Rap1 signaling. Curr Opin Cell Biol 21, 684–693.

Cela C, Llimargas M (2006). EGFR is essential for maintaining epithelial integrity during tracheal remodelling in *Drosophila*. Development 133, 3115–3125.

Chen CM, Freedman JA, Bettler DR Jr, Manning SD, Giep SN, Steiner J, Ellis HM (1996). Polychaetoid is required to restrict segregation of sensory organ precursors from proneural clusters in *Drosophila*. Mech Dev 57, 215–227.

Djiane A, Shimizu H, Wilkin M, Mazleyrat S, Jennings MD, Avis J, Bray S, Baron M (2011). Su(dx) E3-ubiquitin ligase dependent and independent functions of Polychaetoid, the *Drosophila* ZO-1 homologue. J Cell Biol 192, 189–200.

Eckert JJ, Fleming TP (2008). Tight junction biogenesis during early development. Biochim Biophys Acta 1778, 717–728.

Fanning AS, Anderson JM (2009). Zonula occludens-1 and -2 are cytosolic scaffolds that regulate the assembly of cellular junctions. Ann NY Acad Sci 1165, 113–120.

Fehon RG, Dawson IA, Artavanis-Tsakonas S (1994). A *Drosophila* homologue of membrane-skeleton protein 4.1 is associated with septate junctions and is encoded by the *coracle* gene. Development 120, 545–557.

Furuse M (2010). Molecular basis of the core structure of tight junctions. Cold Spring Harb Perspect Biol 2, a002907.

Furuse M, Tsukita S (2006). Claudins in occluding junctions of humans and flies. Trends Cell Biol 16, 181–188.

Gates J, Mahaffey JP, Rogers SL, Emerson M, Rogers EM, Sottile SL, Van Vactor D, Gertler FB, Peifer M (2007). Enabled plays key roles in embryonic epithelial morphogenesis in *Drosophila*. Development 134, 2027–2039.

Gertler F, Doctor J, Hoffman F (1990). Genetic suppression of mutations in the *Drosophila abl* proto-oncogene homolog. Science 248, 857–860.

Ghabrial A, Luschnig S, Metzstein MM, Krasnow MA (2003). Branching morphogenesis of the *Drosophila* tracheal system. Annu Rev Cell Dev Biol 19, 623–647.

Gumbiner B, Stevenson B, Grimaldi A (1988). The role of the cell adhesion molecule uvomorulin in the formation and maintenance of the epithelial junction complex. J Cell Biol 107, 1575–1587.

Harris TJ, Sawyer JK, Peifer M (2009). How the cytoskeleton helps build the embryonic body plan: models of morphogenesis from *Drosophila*. Curr Top Dev Biol 89, 55–85.

Homem CC, Peifer M (2009). Exploring the roles of diaphanous and enabled activity in shaping the balance between filopodia and lamellipodia. Mol Biol Cell 20, 5138–5155.

Ikenouchi J, Umeda K, Tsukita S, Furuse M, Tsukita S (2007). Requirement of ZO-1 for the formation of belt-like adherens junctions during epithelial cell polarization. J Cell Biol 176, 779–786.

Imamura Y, Itoh M, Maeno Y, Tsukita S, Nagafuchi A (1999). Functional domains of alpha-catenin required for the strong state of cadherin-based cell adhesion. J Cell Biol 144, 1311–1322.

Jung AC, Ribeiro C, Michaut L, Certa U, Affolter M (2006). Polychaetoid/ZO-1 is required for cell specification and rearrangement during *Drosophila* tracheal morphogenesis. Curr Biol 16, 1224–1231.

Katsuno T *et al*. (2008). Deficiency of zonula occludens-1 causes embryonic lethal phenotype associated with defected yolk sac angiogenesis and apoptosis of embryonic cells. Mol Biol Cell 19, 2465–2475.

Kiehart DP, Galbraith CG, Edwards KA, Rickoll WL, Montague RA (2000). Multiple forces contribute to cell sheet morphogenesis for dorsal closure in *Drosophila*. J Cell Biol 149, 471–490.

Laplante C, Nilson LA (2006). Differential expression of the adhesion molecule Echinoid drives epithelial morphogenesis in *Drosophila*. Development 133, 3255–3264.

Laplante C, Nilson LA (2011). Asymmetric distribution of Echinoid defines the epidermal leading edge during *Drosophila* dorsal closure. J Cell Biol 192, 335–348.

Laplante C, Paul SM, Beitel GJ, Nilson LA (2010). Echinoid regulates tracheal morphology and fusion cell fate in Drosophila. Dev Dyn 239, 2509–2519.

Larsen CW, Hirst E, Alexandre C, Vincent JP (2003). Segment boundary formation in *Drosophila* embryos. Development 130, 5625–5635.

Larue L, Ohsugi M, Hirchenhain J, Kemler R (1994). E-cadherin null mutant embryos fail to form a trophectoderm epithelium. Proc Natl Acad Sci USA 91, 8263–8267.

Lin HP, Chen HM, Wei SY, Chen LY, Chang LH, Sun YJ, Huang SY, Hsu JC. (2007). Cell adhesion molecule Echinoid associates with unconventional myosin VI/Jaguar motor to regulate cell morphology during dorsal closure in Drosophila. Dev Biol 311, 423–433.

Lindsley DL, Zimm GG (1992). The Genome of *Drosophila melanogaster,* Academic Press: San Diego, CA.

Llimargas M (1999). The Notch pathway helps to pattern the tips of the Drosophila tracheal branches by selecting cell fates. Development 126, 2355–2364.

Lockwood C, Zaidel-Bar R, Hardin J (2008). The *C. elegans* zonula occludens ortholog cooperates with the cadherin complex to recruit actin during morphogenesis. Curr Biol 18, 1333–1337.

McNeil E, Capaldo CT, Macara IG (2006). Zonula occludens-1 function in the assembly of tight junctions in Madin-Darby canine kidney epithelial cells. Mol Biol Cell 17, 1922–1932.

Millard TH, Martin P (2008). Dynamic analysis of filopodial interactions during the zippering phase of *Drosophila* dorsal closure. Development 135, 621–626.

Miyamoto H, Nihonmatsu I, Kondo S, Ueda R, Togashi S, Hirata K, Ikegami Y, Yamamoto D (1995). *canoe* encodes a novel protein containing a GLGF/DHR motif and functions with *Notch* and *scabrous* in common developmental pathways in *Drosophila*. Genes Dev 9, 612–625.

Nelson KS, Furuse M, Beitel GJ (2010). The *Drosophila* claudin Kune-kune is required for septate junction organization and tracheal tube size control. Genetics 185, 831–839.

Nelson WJ (2008). Regulation of cell–cell adhesion by the cadherin–catenin complex. Biochem Soc Trans 36, 149–155.

Oda H, Tsukita S (1999). Nonchordate classic cadherins have a structurally and functionally unique domain that is absent from chordate classic cadherins. Dev Biol 216, 406–422.

Parks AL *et al*. (2004). Systematic generation of high-resolution deletion coverage of the *Drosophila melanogaster* genome. Nat Genet 36, 288–292.

Paul SM, Palladino MJ, Beitel GJ (2007). A pump-independent function of the Na,K-ATPase is required for epithelial junction function and tracheal tube–size control. Development 134, 147–155.

Poulson D (1940). The effect of certain X chromosome deficiencies on the embryonic development of *Drosophila melanogaster*. J Exp Zool 83, 271–325.

Riethmacher D, Brinkmann V, Birchmeier C (1995). A targeted mutation in the mouse E-cadherin results in defective preimplantation development. Genetics 92, 855–859.

Ryder E *et al*. (2004). The DrosDel collection: a set of P-element insertions for generating custom chromosomal aberrations in *Drosophila melanogaster*. Genetics 167, 797–813.

Sawyer JK, Harris NJ, Slep KC, Gaul U, Peifer M (2009). The *Drosophila* afadin homologue Canoe regulates linkage of the actin cytoskeleton to adherens junctions during apical constriction. J Cell Biol 186, 57–73.

Schottenfeld J, Song Y, Ghabrial AS (2010). Tube continued: morphogenesis of the *Drosophila* tracheal system. Curr Opin Cell Biol 22, 633–9.

Seppa MJ, Johnson RI, Bao S, Cagan RL (2008). Polychaetoid controls patterning by modulating adhesion in the *Drosophila* pupal retina. Dev Biol 318, 1–16.

Stevens TL, Rogers EM, Koontz LM, Fox DT, Homem CC, Nowotarski SH, Artabazon NB, Peifer M (2007). Using Bcr-Abl to examine mechanisms by which Abl kinase regulates morphogenesis in *Drosophila*. Mol Biol Cell 19, 378–93.

Suzuki A, Ishiyama C, Hashiba K, Shimizu M, Ebnet K, Ohno S (2002). aPKC kinase activity is required for the asymmetric differentiation of the premature junctional complex during epithelial cell polarization. J Cell Sci 115, 3565–3573.

Takahashi K, Matsuo T, Katsube T, Ueda R, Yamamoto D (1998). Direct binding between two PDZ domain proteins Canoe and ZO-1 and their roles in regulation of the Jun N-terminal kinase pathway in *Drosophila* morphogenesis. Mech Dev 78, 97–111.

Takahisa M, Togashi S, Suzuki T, Kobayashi M, Murayama A, Kondo K, Miyake T, Ueda R (1996). The *Drosophila tamou* gene, a component of the activating pathway of extramacrochaetae expression, encodes a protein homologous to mammalian cell-cell junction-associated protein ZO-1. Genes Dev 10, 1783–1795.

Takai Y, Ikeda W, Ogita H, Rikitake Y (2008). The immunoglobulin-like cell adhesion molecule nectin and its associated protein afadin. Annu Rev Cell Dev Biol 24, 309–342.

Tiklova K, Senti KA, Wang S, Graslund A, Samakovlis C (2010). Epithelial septate junction assembly relies on melanotransferrin iron binding and endocytosis in *Drosophila*. Nat Cell Biol 12, 1071–1077.

Umeda K, Ikenouchi J, Katahira-Tayama S, Furuse K, Sasaki H, Nakayama M, Matsui T, Tsukita S, Furuse M, Tsukita S (2006). ZO-1 and ZO-2 independently determine where claudins are polymerized in tight-junction strand formation. Cell 126, 741–754.

Vincent S, Perrimon N, Axelrod JD (2008). Hedgehog and Wingless stabilize but do not induce cell fate during *Drosophila* dorsal embryonic epidermal patterning. Development 135, 2767–2775.

Wang S, Jayaram SA, Hemphala J, Senti KA, Tsarouhas V, Jin H, Samakovlis C (2006). Septate-junction-dependent luminal deposition of chitin deacetylases restricts tube elongation in the *Drosophila* trachea. Curr Biol 16, 180–185.

Wei SY *et al*. (2005). Echinoid is a component of adherens junctions that cooperates with DE-cadherin to mediate cell adhesion. Dev Cell 8, 493–504.

Wei X, Ellis HM (2001). Localization of the *Drosophila* MAGUK protein Polychaetoid is controlled by alternative splicing. Mech Dev 100, 217–231.

Woolner S, Jacinto A, Martin P (2005). The small GTPase Rac plays multiple roles in epithelial sheet fusion–dynamic studies of *Drosophila* dorsal closure. Dev Biol 282, 163–173.

Wu VM, Schulte J, Hirschi A, Tepass U, Beitel GJ (2004). Sinuous is a *Drosophila* claudin required for septate junction organization and epithelial tube size control. J Cell Biol 164, 313–323.

Wu VM, Yu MH, Paik R, Banerjee S, Liang Z, Paul SM, Bhat MA, Beitel GJ (2007). *Drosophila* Varicose, a member of a new subgroup of basolateral MAGUKs, is required for septate junctions and tracheal morphogenesis. Development 134, 999–1009.

Xu J, Anuar F, Ali SM, Ng MY, Phua DC, Hunziker W (2009). Zona occludens-2 is critical for blood–testis barrier integrity and male fertility. Mol Biol Cell 20, 4268–4277.

Xu J, Kausalya PJ, Phua DC, Ali SM, Hossain Z, Hunziker W (2008). Early embryonic lethality of mice lacking ZO-2, but not ZO-3, reveals critical and nonredundant roles for individual zonula occludens proteins in mammalian development. Mol Cell Biol 28, 1669–1678.

Yamamoto T, Harada N, Kano K, Taya S, Canaani E, Matsuura Y, Mizoguchi A, Ide C, Kaibuchi K (1997). The Ras target AF-6 interacts with ZO-1 and serves as a peripheral component of tight junctions in epithelial cells. J Cell Biol 139, 785–795.

Yamazaki Y, Umeda K, Wada M, Nada S, Okada M, Tsukita S, Tsukita S (2008). ZO-1- and ZO-2-dependent integration of myosin-2 to epithelial zonula adherens. Mol Biol Cell 19, 3801–3811.

Yonemura S, Itoh M, Nagafuchi A, Tsukita S (1995). Cell-to-cell adherens junction formation and actin filament organization: similarities and differences between non-polarized fibroblasts and polarized epithelial cells. J Cell Sci 108, 127–142.